ЯДЕРНА ФІЗИКА
NUCLEAR PHYSICS

УДК 539.1.074.3+524.8 https://doi.org/10.15407/jnpae2019.04.317

R. Bernabei[1,2,*], P. Belli[1,2], F. Cappella[3,4], V. Caracciolo[5], R. Cerulli[1,2], C. J. Dai[6], A. d'Angelo[3,4], A. Di Marco[2], H. L. He[6], A. Incicchitti[3,4], X. H. Ma[6], V. Merlo[1,2], F. Montecchia[2,7], X. D. Sheng[6], Z. P. Ye[6,8]

[1] Dipartimento di Fisica, Università di Roma "Tor Vergata", Rome, Italy
[2] INFN, sez. Roma "Tor Vergata", Rome, Italy
[3] Dipartimento di Fisica, Università di Roma "La Sapienza", Rome, Italy
[4] INFN, sez. Roma, Rome, Italy
[5] INFN Laboratori Nazionali del Gran Sasso, Assergi, Italy
[6] Key Laboratory of Particle Astrophysics, Institute of High Energy Physics, Chinese Academy of Sciences, Beijing, P.R. China
[7] Dipartimento Ingegneria Civile e Ingegneria Informatica, Università di Roma "Tor Vergata", Rome, Italy
[8] University of Jinggangshan, Ji'an, Jiangxi, P.R. China

*Corresponding author: rita.bernabei@roma2.infn.it

IMPROVED MODEL-DEPENDENT COROLLARY ANALYSES AFTER THE FIRST SIX ANNUAL CYCLES OF DAMA/LIBRA-phase2

Several of the many proposed Dark Matter candidate particles, already investigated with lower exposure and a higher software energy threshold, are further analyzed including the first DAMA/LIBRA-phase2 data release, with an exposure of 1.13 t·yr and a lower software energy threshold (1 keV). The cumulative exposure above 2 keV considering also DAMA/NaI and DAMA/LIBRA-phase1 results is now 2.46 t·yr. The analysis permits to constrain the parameters' space of the considered candidates restricting their values – with respect to previous analyses – thanks to the increase of the exposure and to the lower energy threshold.

Keywords: Dark Matter, elementary particle processes, scintillation detectors.

1. Introduction

The model-independent results of the first six full annual cycles measured by DAMA/LIBRA-phase2 with software energy threshold lowered down to 1 keV[1] [1, 2] have been released [3 - 7]. On the basis of the exploited Dark Matter (DM) annual modulation signature, the model-independent evidence for the presence of DM particles in the galactic halo has been further confirmed after the previous DAMA/LIBRA-phase1 [8 - 11, 1, 2, 12 - 14] and the former DAMA/NaI [15, 16]; the cumulative C.L. is increased from the previous 9.3 σ (data from 14 independent annual cycles: cumulative exposure 1.33 t·yr) to 12.9 σ (data from 20 independent annual cycles: cumulative exposure 2.46 t·yr)[2].

The expected differential counting rate of DM particles depends on the Earth's velocity in the galactic frame, which depends on the time: $v_E(t) = v_\odot + v_\oplus \cos\gamma \cos\omega(t - t_0)$. Here $v_\odot$ is the Sun velocity with respect to the galactic halo ($v_\odot \simeq v_0 + 12$ km/s and v_0 is the local velocity), $v_\oplus \simeq$ 30 km/s is the Earth's orbital velocity around the Sun on a plane with inclination γ = 60° with respect to the galactic plane. Furthermore, ω= 2π/T with T = 1 yr and roughly $t_0 \simeq$ June 2nd (when the Earth's speed in the galactic halo is at maximum). Hence, the expected counting rate averaged in a given energy interval can be conveniently worked out through a first-order Taylor expansion:

$$S(t) = S_0 + S_m \cos\omega(t - t_0), \qquad (1)$$

with the contribution from the highest order terms being less than 0.1 %; S_m and S_0 are the modulation amplitude and the un-modulated part of the expected differential counting rate, respectively.

Since in DAMA experiments the model-independent DM annual modulation signature is exploited, the experimental observable is the modulation amplitude, S_m, as a function of the energy, and the identification of the constant part of the signal, S_0, is not required as opposed to other methods. This approach has several advantages; in particular, the only background of interest is the one able to mimic the signature, i.e. able to account for the whole

[1] Throughout this paper keV means keV electron equivalent, where not otherwise specified.
[2] Throughout this paper ton means metric ton (1000 kg).

observed modulation amplitude and to simultaneously satisfy all the many specific peculiarities of this signature (see e.g. Ref. [5]). No background of this sort has been found or suggested by anyone over some decades, see Refs. [2 - 13]; in particular, in the latter two references the case of neutrons, muons, and solar neutrinos have further been addressed in detail[3]. Noteworthy, as already pointed out in Refs. [17, 18], this signature acts as an efficient background rejection procedure and does not require any identification of S_0 from the total counting rate in order to establish the presence of DM particles in the galactic halo. Therefore, the DM annual modulation signature allows one to overcome – in the identification of the existence of a signal – the large uncertainties associated to: i) many statistical data selections/subtractions/discrimination procedures; ii) strongly uncertain modeling of the background, in particular in keV region; iii) *a priori* assumption on the nature, interaction type, etc. of the DM particle(s). On the other hand, it requires uncontested stability at the level of less than 1% of the operational experimental parameters.

In Table 1 the experimental modulation amplitudes, S_m, measured by DAMA/NaI, DAMA/LIBRA-phase1 and DAMA/LIBRA-phase2 are shown; the data below 2 keV refer, instead, only to the DAMA/LIBRA-phase2 [5].

The aim of the present paper is to update the implications on several models (of the many available in the literature) we already investigated with lower exposure and higher software energy threshold with the data previously collected with DAMA/NaI and DAMA/LIBRA-phase1.

Table 1. **Experimental modulation amplitudes, S_m, measured by DAMA/NaI, DAMA/LIBRA-phase1 and DAMA/LIBRA-phase2 (total exposure 2.46 t·yr); data below 2 keV refer, instead, only to the DAMA/LIBRA-phase2 (exposure 1.13 t·yr) [5]**

Energy, keV	S_m, cpd/kg/keV	Energy, keV	S_m, cpd/kg/keV
(1.0 - 1.5)	(0.0232 ± 0.0052)	(6.5 - 7.0)	(0.0016 ± 0.0018)
(1.5 - 2.0)	(0.0164 ± 0.0043)	(7.0 - 7.5)	(0.0007 ± 0.0018)
(2.0 - 2.5)	(0.0178 ± 0.0028)	(7.5 - 8.0)	(0.0016 ± 0.0018)
(2.5 - 3.0)	(0.0190 ± 0.0029)	(8.0 - 8.5)	(0.0014 ± 0.0018)
(3.0 - 3.5)	(0.0178 ± 0.0028)	(8.5 - 9.0)	(0.0029 ± 0.0018)
(3.5 - 4.0)	(0.0109 ± 0.0025)	(9.0 - 9.5)	(0.0014 ± 0.0018)
(4.0 - 4.5)	(0.0110 ± 0.0022)	(9.5 - 10.0)	–(0.0029 ± 0.0019)
(4.5 - 5.0)	(0.0040 ± 0.0020)	(10.0 - 10.5)	(0.0035 ± 0.0019)
(5.0 - 5.5)	(0.0065 ± 0.0020)	(10.5 - 11.0)	–(0.0038 ± 0.0019)
(5.5 - 6.0)	(0.0066 ± 0.0019)	(11.0 - 11.5)	–(0.0013 ± 0.0019)
(6.0 - 6.5)	(0.0009 ± 0.0018)	(11.5 - 12.0)	–(0.0019 ± 0.0019)

The plan of the paper is as follows. In Sect. 2 the description of the data analysis and the inclusion of the uncertainties used in the evaluation of the allowed regions are described. In Sect. 3 the results achieved for the considered scenarios of DM particles are reported: i) DM particles which elastically interact with target nuclei with Spin-Independent (SI) or Spin-Dependent (SD) or mixed-coupling (Sect. 3.1); ii) DM particles with preferred electron interaction (Sect. 3.2); iii) DM particles with preferred inelastic scattering (Sect. 3.3); iv) Light DM (Sect. 3.4); v) asymmetric and symmetric Mirror DM (Sect. 3.5). Moreover, some of the many other interesting scenarios available in the literature are introduced for the first time. Finally, Sect. 4 is devoted to our conclusions.

2. Data analysis

As mentioned the corollary analyses presented here are model-dependent; thus, it is important to point out at least the main topics which enter in the determination of results and the related uncertainties. These arguments have been already addressed at various extents in previous corollary model-dependent analyses. The DM candidates considered here have been previously discussed in the Refs. [2, 15, 16, 19 - 30].

As first, in order to derive the allowed regions of the parameter's space of the DM particles in the considered scenarios, a specific phase-space distribution function (DF) of each DM candidate in the galactic halo has to be adopted. A large number of

[3] Concerning recently appeared remarks, let us comment that any hypothetical effect due to environmental Helium diffusion inside the photomultipliers (PMTs) can be excluded, even considering the following simple arguments [7]: i) the PMTs are kept in high purity (HP; 5.5 grade) Nitrogen atmosphere, the gas being continuously flushed through the apparatus (≃ 250 liters/hour) [8]; thus no Helium accumulation process can take place (typical characteristic time for accumulation of Helium in PMTs through glass – considering the permeability of the materials – is ≃ 1 yr). An estimate of Helium concentration within the DAMA shield is less than $5 \cdot 10^{-11}$ ppm. Thus, any hypothetical effect due to He-correlated events is negligible; ii) any migration of Helium into PMTs would cause their irreversible degradation which has not been observed: e.g. the dark noise of the PMTs ranges from 40 to 500 Hz [1] and improves over time on the contrary of what it is expected by any hypothetical He migration inside PMTs; iii) the PMTs used in DAMA/LIBRA-phase2 and DAMA/LIBRA-phase1 are different and with different voltage values on the first dynode; in the He erroneous conjecture this should have produced different modulation amplitudes in the two phases, which has not been observed; iv) this conjecture needs that the He is modulated and with the same phase and period as the dark matter, but getting the right phase and period over 20 annual cycles is practically excluded.

possibilities are available in the literature; these models are continuously in evolution thanks to the new simulations and new astrophysical observations, as the recent GAIA ones (see e.g. Refs. [31, 32] and references therein). Thus, large uncertainties in the predicted theoretical rate are present.

In this paper, to account to some extent for the uncertainties in halo models, we consider the same not-exhaustive set of halo models as in our previous published analyses [15, 16, 24], for all the considered DM candidates. This can give an idea of the role of some astrophysical uncertainties on DM model-dependent analyses and offers a direct impact on the increase of the exposure and of the lowering of the software energy threshold, achieved with DAMA/LIBRA-phase2. Further analyses in other frameworks, such as e.g. exploiting recent GAIA data, can be possible in dedicated future papers. The considered models are summarized in Table 2. In particular, the considered classes of halo models correspond to: (1) spherically symmetric matter density with isotropic velocity dispersion (Class A); (2) spherically symmetric matter density with non-isotropic velocity dispersion (Class B); (3) axisymmetric models (Class C); (4) triaxial models (Class D); (5) moreover, in the case of axisymmetric models it is possible to include either a halo co-rotation or a halo counter-rotation.

Table 2. **Summary of the considered consistent halo models [24, 15]. The labels in the first column identify the models. In the third column, the values of the related considered parameters are reported [24, 15]; other choices are also possible as well as other halo models. The models of Class C have also been considered including possible co-rotation and counter-rotation of the dark halo.**

Class A: spherical ρ_{dm}, isotropic velocity dispersion		
A0	Isothermal Sphere	
A1	Evans' logarithmic	R_c = 5 kpc
A2	Evans' power-law	R_c = 16 kpc, β = 0.7
A3	Evans' power-law	R_c = 2 kpc, β = –0.1
A4	Jaffe	α = 1, β = 4, γ = 2, a = 160 kpc
A5	NFW	α = 1, β = 3, γ = 1, a = 20 kpc
A6	Moore et al.	α = 1.5, β = 3, γ = 1.5, a = 28 kpc
A7	Kravtsov et al.	α = 2, β = 3, γ = 0.4, a = 10 kpc
Class B: spherical ρ_{dm}, non-isotropic velocity dispersion (Osipkov - Merrit, β_0 = 0.4)		
B1	Evans' logarithmic	R_c = 5 kpc
B2	Evans' power-law	R_c = 16 kpc, β = 0.7
B3	Evans' power-law	R_c = 2 kpc, β = –0.1
B4	Jaffe	α = 1, β = 4, γ = 2, a = 160 kpc
B5	NFW	α = 1, β = 3, γ = 1, a = 20 kpc
B6	Moore et al.	α = 1.5, β = 3, γ = 1.5, a = 28 kpc
B7	Kravtsov et al.	α = 2, β = 3, γ = 0.4, a = 10 kpc
Class C: Axisymmetric ρ_{dm}		
C1	Evans' logarithmic	R_c = 0, $q = 1/\sqrt{2}$
C2	Evans' logarithmic	R_c = 5 kpc, $q = 1/\sqrt{2}$
C3	Evans' power-law	R_c = 16 kpc, q = 0.95, β = 0.9
C4	Evans' power-law	R_c = 2 kpc, $q = 1/\sqrt{2}$, β = –0.1
Class D: Triaxial ρ_{dm} (q = 0.8, ρ = 0.9)		
D1	Earth on maj. axis, rad. anis.	δ = –1.78
D2	Earth on maj. axis, tang. anis.	δ = 16
D3	Earth on interm. axis, rad. anis.	δ = –1.78
D4	Earth on interm. axis, tang. anis.	δ = 16

In our analysis we also consider the physical ranges of the main halo parameters: the local total DM density, ρ_0, and the local velocity v_0 as discussed in Ref. [24]. The range of the possible v_0 values is from 170 to 270 km/s. For ρ_0, its minimal, ρ_0^{min}, and its maximal, ρ_0^{max}, values are estimated imposing essentially two astrophysical constraints: one on the amount of non-halo components and the other on the flatness of the rotational curve in the Galaxy; for a detailed procedure see Ref. [24].

The values for ρ_0^{min} and ρ_0^{max} are related to the DF and the considered v_0; they are reported in Table

III of Ref. [24]. The halo density ρ_0 ranges from 0.17 to 0.67 GeV/cm^3 for v_0 = 170 km/s, while ρ_0 ranges from 0.29 to 1.11 GeV/cm^3 for v_0 = 220 km/s, and ρ_0 ranges from 0.45 to 1.68 GeV/cm^3 for v_0 = = 270 km/s, depending on the halo model.

To take into account that the considered DM candidate can be just one of the components of the dark halo, the ξ the parameter is introduced; it is defined as the fractional amount of local density in terms of the considered DM candidate ($\xi \leq 1$). Thus, the local density of the DM particles is $\rho_{DM} = \xi\rho_0$.

Finally, we consider the DM escape velocity, v_{esc}, from the galactic gravitational potential; actually, it is also affected by significant uncertainty: (528^{+24}_{-25}) km/s [33], 498 < v_{esc} < 608 km/s (90 % C.L.), with a median likelihood of 544 km/s [34], (533^{+54}_{-41}) km/s (90 % C.L.) [35], (521^{+46}_{-30}) km/s [36], and (580±63) km/s [37]. In the following analysis v_{esc} = = 550 km/s is adopted, as often considered in the literature. However, no sizable differences are observed in the final results when v_{esc} values ranging from 550 to 650 km/s are considered. In particular, for low-mass DM particles scattering off nuclei, the Na contribution is dominant and has a small dependence on the tail of the velocity distribution.

In addition, it is also possible the presence of non-virialized components, like streams in the dark halo coming from external sources with respect to our Galaxy [26, 38, 39] or other scenarios as e.g. that of Ref. [40 - 42]; however, these latter possibilities are not included in the present analyses.

In conclusion, to properly evaluate the allowed regions in the parameters' space of particle DM scenarios it is limiting only considering an isothermal profile[4] with local parameters v_0 = 220 km/s and ρ_0 = 0.3 GeV/cm^3 without taking in consideration at least some of the other existing possibilities in the distribution of velocity and spatial coordinates permitted by astrophysical observations.

In the interaction of DM particles in the NaI(Tl) detectors the detected energy, E_{det}, is a key quantity. It is connected with the energy released by the products of the interaction, E_{rel}; two possibilities exist: 1) the products of the interaction have electromagnetic nature (mainly electrons); 2) a nuclear recoil with E_R kinetic energy is produced by the DM particle scattering either off Sodium or off Iodine nucleus. Since the detectors are calibrated by γ sources, in the first case $E_{det} = E_{rel}$, while in the second case a quenching factor for each recoiling nucleus must be included: $E_{det} = q_{Na,I} \cdot E_{rel}$. For completeness, we also recall that the energy resolutions of each detector in the two configurations (phase1 and phase2) are shown e.g. in Ref. [1].

2.1. The case of DM particles inducing nuclear recoils

The quenching factors are a property of the specific detector and not general properties of any NaI(Tl), particularly in the very low energy range. In fact, in NaI(Tl) they depend on the adopted growing procedures, on Tl concentration and uniformity in the detector, on the specific additives always used by companies to strengthen the performance of the detectors, on the monocrystalline or polycrystalline nature of the NaI(Tl) crystal, etc. Moreover, their measurements are difficult and always affected by significant experimental uncertainties. All these aspects are always relevant sources of uncertainties when comparing whatever results in terms of DM candidates inducing nuclear recoils. Naively summarizing, different quenching factors values imply that the same energy in keV electron equivalent corresponds to different recoil energies in the different experiments.

Arguments on various quenching factors determinations have already been addressed by us e.g. in Refs. [15, 19 - 21, 30]. It is worth noting that recently Ref. [45] gave quenching factors for a small COSINE-100 like detector; in particular: Na quenching factor ranging from 0.1 to 0.23 with a significant energy dependence, and I quenching factor ranging from 0.04 to 0.06 were reported; a very high precision is quoted. However, these values cannot be consistently considered for other detectors because of the above-mentioned arguments; in particular, those crystals have been grown by different techniques and protocols than those of DAMA/LIBRA. For example, the energy of the internal α's in those detectors roughly ranges between 2.3 and 3.0 MeV electron equivalent [46], while in DAMA/LIBRA it ranges between 2.6 and 4.5 MeV electron equivalent [8], indicating a lower quenching factor for α's in COSINE-100 like detectors; thus, much lower quenching factors at keV region are implied as well.

In literature, one can find a lot of measurements on the Na and I quenching factors that, owing to the above considerations, show a wide spread. It is evident also in Fig. 10 of Ref. [45], where

[4] It is also worth noting that the isothermal halo is an unphysical model; for example, the mass would diverge and one has to adopt a by-hand cut-off. Let us remark, however, that flat density profile for the Galaxy within the radius of 10 kpc can be obtained if the DM particles have self-interaction cross section $\sigma/M \simeq 10^{-24} - 10^{-23}$ cm^2/GeV [43, 44].

systematically poorer quenching factors are obtained for crystals recently developed (with different techniques and materials) with respect to previous measurements[5].

In the following the same procedures previously adopted in Refs. [19 - 21, 30] are considered. This also allows us to point out – by direct comparison with previously published results – the effect of increasing the exposure and decreasing the energy threshold. Three possible instances can be considered:

(Q_I) quenching factors of Na and I "constants" with respect to the recoil energy E_R: the adopted values are q_{Na} = 0.3 and q_I = 0.09, measured with neutron source integrating the data over the 6.5 - 97 keV and the 22 - 330 keV recoil energy range, respectively [49];

(Q_{II}) quenching factors varying as a function of E_R evaluated as in Ref. [50];

(Q_{III}) quenching factors with the same behavior of Ref. [50], but normalized in order to have their mean values consistent with (Q_I) in the energy range considered there.

Moreover, to account for the uncertainties on the measured quenching factors some discrete cases of possibilities will also be introduced at the end of this Section. For a long time in the field, the quenching factors have been considered locally constant with energy. On the contrary, the (Q_{II}), (Q_{III}) instances use energy-dependent quenching factors following the phenomenological prescription of Ref. [50].

Another important effect is the channeling of low energy ions along axes and planes of the NaI(Tl) DAMA crystals. This effect can lead to a further important deviation, in addition to the uncertainties discussed in section II of Ref. [19] and in Ref. [20]. In fact, the channeling effect in crystals implies that a fraction of nuclear recoils is channeled and experience much larger quenching factors than those derived from neutron calibration (see Refs. [28, 19] for a discussion of these aspects). Anyhow, the channeling effect in solid crystal detectors is not a well-fixed issue. There could be several uncertainties in the modeling. Moreover, the experimental approaches (as that in Ref. [51]) are rather difficult since the channeled nuclear recoils are – even in the most optimistic model – a very tiny fraction of the not-channeled ones. In particular, the modeling of the channeling effect described in Ref. [28], where the recoiling nuclei are considered free in the lattice, is able to reproduce the recoil spectrum measured at the neutron beam by some other groups [28]. For completeness, we mention: i) the alternative channeling model of Ref. [52], where larger probabilities of the planar channeling are expected; ii) the analytic calculation of Ref. [53], where it is claimed that the channeling effect holds for recoils coming from outside a crystal and not from recoils from lattice sites, due to the blocking effect. Nevertheless, although some amount of blocking effect could be present, the precise description of the crystal lattice with dopant and trace contaminants is quite difficult and analytical calculations require some simplifications, which can affect the result. Because of the difficulties of experimental measurements and of the theoretical estimate of the channeling effect, in the following, it will be either included using the procedure given in Ref. [28] or not in order to give an idea of the related uncertainty.

In the case of low mass DM particles giving rise to nuclear recoils, the Migdal effect (discussed in detail in Refs. [27, 20], where the impact in some corollary analyses was discussed) can also be considered.

Finally, some discrete cases are considered in the following to cautiously account for possible uncertainties on the quenching factors measured by DAMA in its detectors and on the parameters used in the SI and SD nuclear form factors, as already done in previous analyses. Three cases are considered:

- set A considers the mean values of the parameters of the used nuclear form factors [15] and of the quenching factors;

- set B adopts the same procedure as in Refs. [54, 23, 16], by varying (i) the mean values of the ^{23}Na and ^{127}I quenching factors as measured in Ref. [49] up to +2 times the errors; (ii) the nuclear radius, r_A, and the nuclear surface thickness parameter, s, in the SI nuclear form factor from their central values down to −20 %; (iii) the b parameter in the considered SD nuclear form factor from the given value down to −20 %;

- set C where the Iodine nucleus parameters are fixed at the values of set B, while for the Sodium nucleus one considers [15]: (i) ^{23}Na quenching factor at q_{Na} = 0.25[6]; (ii) the nuclear radius, r_A, and the nuclear surface thickness parameter, s, in the SI nuclear form factor from their central values up to +20 %; (iii) the b parameter in the considered SD nuclear form factor from the given value up to +20 %.

[5] For example, Ref. [47] reports Na quenching factor substantially constant with energy and significantly higher than Ref. [45] with a very good precision as well. Moreover, Ref. [45] claims agreement with Ref. [48], but this latter reference gives mean values systematically higher.

[6] This value offers backward compatibility with previous similar model-dependent DAMA studies and a safe realistic representation of possible uncertainties in the q_{Na} measured for the DAMA detectors.

2.2. The analysis procedure

Model-dependent corollary analyses through a maximum likelihood procedure, which also takes into account the energy behavior of each detector, can be pursued.

In the following for each considered scenario, the allowed domains in the corresponding parameters' space will be obtained by marginalizing over the halo models of Table 2, over halo parameters (v_0 and ρ_0) and over the sets A, B, C[7]. This procedure shows the impact of the uncertainties in the astrophysical, nuclear and particle physics on the model-dependent analyses.

However, for simplicity, the allowed regions in the parameters' space of each considered scenario can also be derived by comparing – for each *k-th* energy bin of 1 keV – the measured DM annual modulation amplitude, $S^{exp}_{m,k} \pm \sigma_k$ [8], with the theoretical expectation in each considered framework, $S^{th}_{m,k}$. Of course, the $S^{th}_{m,k}$ values depend on the free parameters of the model $\bar{\theta}$, such as the DM particle mass, the cross-section, etc., on the uncertainties accounted for, on the proper accounting for the detector's features, and on priors.

As mentioned in previous works (as e.g. recently in Refs. [20, 21]), a cautious prior on $S_{0,k}$ – assuring safe and more realistic allowed regions/volumes – can be worked out from the measured counting rate in the cumulative energy spectrum; the latter is given by the sum of the un-modulated background contribution b_k (whose existence is shown by the detailed analyses on residual radioactive contaminations in the detectors [8]) and of the constant part of the signal $S_{0,k}$. By adopting a standard procedure, used in the past in several low background fields, one can derive lower limits on b_k and, thus, upper limits on $S_{0,k}$ ($S^{max}_{0,k}$). In particular, in DAMA/LIBRA-phase2 is obtained: $S_0 \lesssim 0.80$ cpd/kg/keV in the (1–2) keV energy interval; $S_0 \lesssim 0.24$ cpd/kg/keV in (2–3) keV, and $S_0 \lesssim 0.12$ cpd/kg/keV in (3–4) keV[9].

Thus, the following χ^2 can be calculated for each considered model:

$$\chi^2(\bar{\theta}) = \sum_k \frac{(S^{exp}_{m,k} - S^{th}_{m,k}(\bar{\theta}))^2}{\sigma_k^2} + \sum_{k'} \frac{(S^{max}_{0,k'} - S^{th}_{0,k'}(\bar{\theta}))^2}{\sigma^2_{0,k'}} \Theta(S^{th}_{0,k'}(\bar{\theta}) - S^{max}_{0,k'}), \quad (2)$$

where the second term encodes the experimental bounds about the un-modulated part of the signal; 10^{-3} cpd/kg/keV, Θ is the Heaviside function, and $S^{th}_{0,k'}$ is the average expected signal counting rate in the k' energy bin. The sum in the first term in Eq. (2) runs here from 1 keV to 20 keV.

The χ^2 defined in Eq. (2) can be calculated in each considered framework and is a function of the model parameters $\bar{\theta}$. Thus, we can define:

$$\Delta\chi^2(\bar{\theta}) = \chi^2(\bar{\theta}) - \chi^2_0, \quad (3)$$

where χ^2_0 is the χ^2 for $\bar{\theta}$ values corresponding to the absence of signal. The $\Delta\chi^2$ is used to determine the allowed intervals of the model parameters $\bar{\theta}$ at 10 σ from the *null signal hypothesis*.

It is worth noting that the results presented in the following are, of course, not exhaustive of the many possible scenarios. For example, the possible contribution of the non-thermalized component in the Dark Halo, which would extend the allowed regions of the DM particle's parameters, is not included in the present paper.

Moreover, the improvement in the energy threshold achieved by DAMA/LIBRA-phase2 at 1 keV prevents to find configurations due to the Migdal effects, which were instead present with the 2 keV energy threshold data. This is an example of the relevance of lowering the energy threshold to disentangle at least among some of the possible scenarios.

Finally, we have verified that the Q_{III} option for the quenching factors provides results similar to the case of the Q_I option; thus, to avoid the overloading of the figures in the following the Q_{III} case is not considered.

3. Updated corollary model-dependent scenarios

In the following we will present the updated results for DM candidates in the frameworks described above, using the total exposure of 2.46 t·yr for the data from 2 to 6 keV and of 1.13 t·yr for the data below 2 keV.

[7] In particular, each allowed domain encloses all the allowed regions obtained for each chosen configuration of model and parameters.

[8] The distributions of the measured modulation amplitudes around their mean value show a perfect Gaussian behaviors, justifying the use of a symmetric uncertainty [9, 2, 11, 3, 5].

[9] Disregarding this prior is one of the main critical issues in model-dependent analyses by other authors.

3.1. DM particles elastically interacting with target nuclei

A lot of candidates have been proposed in theory extending the Standard Model of particles that includes candidates for Dark Matter elastically scattering off target nuclei.

In the DM particle-nucleus, elastic scattering, the differential energy distribution of the recoil nuclei can be calculated by means of the differential cross-section of the DM-nucleus elastic process [49, 22, 15, 16, 28]. The latter is given by the sum of two contributions: the SI and the SD one.

In the purely SI case, the nuclear parameters can be decoupled from the particle parameters and the nuclear cross-sections, which are derived quantities, are usually scaled to a defined point-like SI DM particle-nucleon cross-section, σ_{SI}. In principle, this procedure could allow – within a framework of several other assumptions (that in turn introduce uncertainties in final evaluations) – a model-dependent comparison among different target nuclei, otherwise impossible. In the following, the usually considered coherent scaling law for the nuclear cross-sections is adopted:

$$\sigma_{SI}(A,Z) \propto m_{red}^2(A,DM)[f_p Z + f_n(A-Z)]^2, \quad (4)$$

where $\sigma_{SI}(A,Z)$ is the point-like cross-section of DM particles scattering off nuclei of mass number A and atomic number Z, $m_{red}(A,DM)$ is the reduced mass of the system of DM particle and nucleus, f_p and f_n are the effective DM particle couplings to protons and neutrons, respectively. The case of isospin violation $f_p \neq f_n$ will be discussed in Sect. 3.1.2; now we assume $f_p = f_n$ and, thus, we can write[10]:

$$\sigma_{SI}(A,Z) = \frac{m_{red}^2(A,DM)}{m_{red}^2(1,DM)} A^2 \sigma_{SI} \quad (5)$$

As for nuclear SI form factors, the Helm form factor [56, 57] has been adopted[11]. Details on the used form factors can also be found in Ref. [15]. As described above, some uncertainties on the nuclear radius and on the nuclear surface thickness parameters in the Helm SI form factors have been included in the following analysis by considering three discrete cases, labeled as set A, B, and C in Sect. 2.1.

The purely SD case is even more uncertain since the nuclear and particle physics degrees of freedom cannot be decoupled and a dependence on the assumed nuclear potential exists. Also in the purely SD case, all the nuclear cross-sections are usually scaled to a defined point-like SD Dark Matter particle-nucleon cross-section, σ_{SD} [54, 15]. The adopted scaling law for this case profits of the proportionality of the SD nuclear cross-section to the nuclear spin factor $\Lambda^2 J(J+1)$ and to the squared reduced mass. To take into account the finiteness of the nucleus, a SD nuclear form factor is also used; for details of its parametrization used in the following see Ref. [15]. A further parameter must be introduced; in fact, following the notations reported in Ref. [54]: $\tan\theta = a_n/a_p$, where $a_{p,n}$ are the effective DM-nucleon coupling strengths for SD interactions. The mixing angle θ is defined in the $[0, \pi)$ interval; in particular, θ values in the second sector account for a_p and a_n with different signs. Therefore, further significant uncertainties in the evaluation of the SD interaction rate also arise from the adopted spin factor for the single target-nucleus. In fact, the available calculated values are well different in different models (and differently vary for each nucleus) and, in addition, at the fixed model they depend on θ [54, 15].

It is worth noting that for the SD part of the interaction not only the target nuclei should have spin different from zero (for example, this is not the case of Ar isotopes, and most of the Ca, Ge, Te, Xe, W isotopes) to be sensitive to DM particles with a SD component in the coupling, but also well different sensitivities can be expected among odd-nuclei having an unpaired proton (as e.g. ^{23}Na and ^{127}I, and ^{1}H, ^{19}F, ^{27}Al, ^{133}Cs) and odd-nuclei having an unpaired neutron (as e.g. the odd Xe and Te isotopes and ^{29}Si, ^{43}Ca, ^{73}Ge, ^{183}W).

In conclusion, the free parameters once fixed the assumptions for the model framework, are the DM particle mass, m_{DM}, the $\xi\sigma_{SI}$ for the purely SI case, the $\xi\sigma_{SD}$ and θ for the purely SD case. Therefore, in the SI case, the allowed regions are presented in the plane $\xi\sigma_{SI}$ vs m_{DM}, while in the SD case $\xi\sigma_{SD}$, θ and m_{DM} give rise to the 3-dimensional allowed volume of which generally only slices in the plane $\xi\sigma_{SD}$ vs m_{DM} are depicted at fixed θ values. Obviously, the situation is even more complex when the SI and SD mixed case is considered and both the large uncertainties existing for the SI and SD interactions are present. In this general scenario the data give rise to an allowed volume in the

[10] It was also proposed that two-nucleon currents from pion exchange in the nucleus can give different contribution for nuclei with different atomic number [55], as a consequence the cross section for some nuclei can be enhanced with respect to others. Also similar arguments have a great relevance in the model-dependent comparisons.

[11] It should be noted that the Helm form factor is the least favorable one e.g. for Iodine and requires larger SI cross sections for a given signal rate; in case other form factor profiles, considered in the literature, would be used, the allowed parameters' space would extend [15].

4-dimensional space (m_{DM}, $\xi\sigma_{SI}$, $\xi\sigma_{SD}$, θ); practically just some slices of this 4-dimensional allowed volume in the plane $\xi\sigma_{SI}$ vs $\xi\sigma_{SD}$ for some of the possible θ and m_{DM} values in some of the possible model frameworks are depicted.

3.1.1. Spin-Independent interaction

Often the purely SI interaction with ordinary matter is assumed to be dominant.

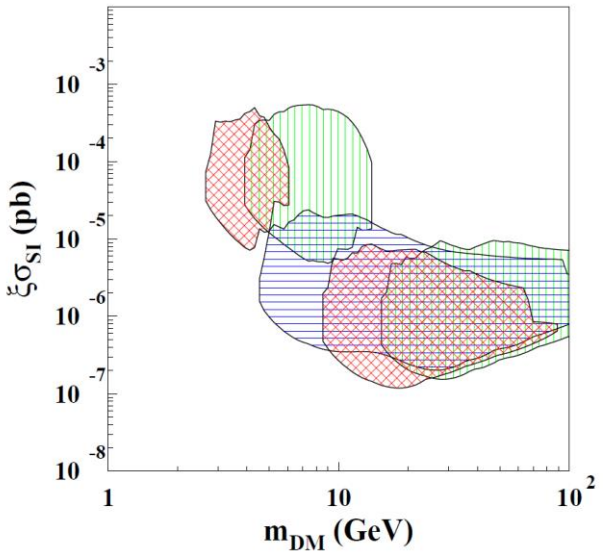

Fig. 1. Regions in the nucleon cross-section vs DM particle mass plane allowed by DAMA experiments in the case of a DM candidate elastically scattering off target nuclei and SI interaction. Three different instances for the Na and I quenching factors have been considered: (i) Q_I case [(green on-line) vertically-hatched region], (ii) with channeling effect [(blue on-line) horizontally-hatched region)] and (iii) Q_{II} [(red on-line) cross-hatched region]. The regions have been obtained by marginalizing all the models for each considered scenario (see Sect. 2) and they represent the domain where the likelihood-function values differ more than 10 σ from the *null hypothesis* (absence of modulation). (See color Figure on the journal website.)

In addition, most of the used target-nuclei are practically not sensitive to SD interactions (on the contrary to ^{23}Na and ^{127}I) and the theoretical calculations and comparisons are even much more complex and uncertain. Therefore, for the purely SI scenario in the considered model frameworks the allowed region in the plane m_{DM} and $\xi\sigma_{SI}$ have been calculated and shown in Fig. 1. Of course, best-fit values of cross-section and DM mass span over a large range in the considered model frameworks.

The allowed domains in Fig. 1 are obtained by marginalizing all the models for each considered scenario (see Sect. 2); they represent the domains where the likelihood-function values differ more than 10 σ from the absence of signal. The three different instances described above for the Na and I quenching factors have been considered: (i) Q_I case, (ii) with channeling effect, and (iii) Q_{II}.

When comparing with the previous results obtained only considering DAMA/NaI [15] and DAMA/LIBRA-phase1 [11] data, one can derive that: 1) the C.L. associated to the regions allowed in the described frameworks is improved; 2) the allowed regions are restricted (i.e. several configurations for the specifically considered frameworks are no more supported by the cumulative data at the given C.L.); 3) in the Q_I and Q_{II} cases the low and high mass regions, driven by the Na and I nuclei, respectively, are disconnected; 4) including the channeling effect the lower available mass is 4 GeV, instead of 2 GeV as in the previous analysis [19, 2].

In Fig. 2 few examples of superposition of the measured S_m^{exp} vs energy (points with error bars) with theoretical expectations (solid histograms) for SI case are shown. In general, the comparison for most of the considered scenarios is very stringent when the channeling effect is included according to Ref. [28] as in the examples shown in Fig. 3. In these examples, the Evans logarithmic halo model has been considered. We recall that the Evans model is an analytical solution giving the DF for particular families of logarithmic gravitational potentials related to the total matter distribution in the Galaxy. Hereafter, the theoretical expectations are reported below 1 keV to show the importance of further lowering the energy threshold to disentangle among the different models and scenarios.

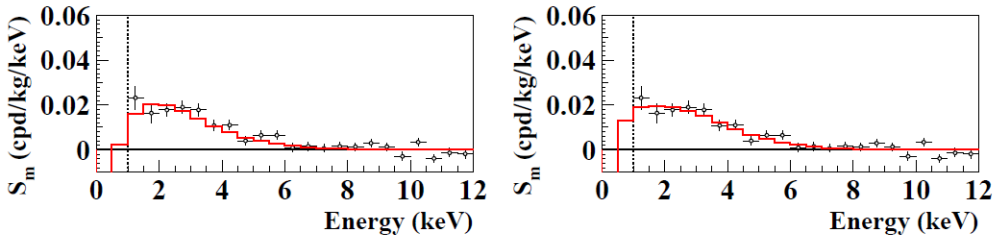

Fig. 2. Examples of superposition of the measured S_m^{exp} vs energy (points with error bars) with theoretical expectations (solid histograms) for the SI case with quenching factors Q_I. *Left*: case of the A1 (Evans logarithmic) halo model with ρ_0 = 0.2 GeV/cm^3, v_0 = 170 km/s and set B of parameters values; *Right*: case of the C2 (Evans logarithmic) halo model with ρ_0 = 0.67 GeV/cm^3, v_0 = 170 km/s and set C of parameters values. In both cases the mass of the DM particle is 60 GeV and $\xi\sigma_{SI}$ is equal to $3.9\cdot10^{-6}$ pb and to $1.3\cdot10^{-6}$ pb, respectively. (See color Figure on the journal website.)

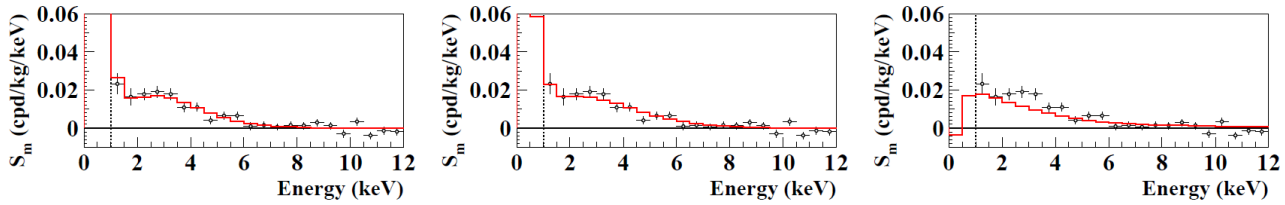

Fig. 3. Examples of superposition of the measured S_m^{exp} vs energy (points with error bars) with theoretical expectations (solid histograms) for the SI case, when the channeling effect is included [28]. *Left*: case of the C1 (Evans logarithmic) halo model with ρ_0 = 0.56 GeV/cm^3, v_0 = 170 km/s, set A of parameters values, DM particle mass 14 GeV and $\xi\sigma_{SI}$ equal to 5.5·10^{-6} pb. *Center*: case of the C2 (Evans logarithmic) halo model with ρ_0 = 0.67 GeV/cm^3, v_0 = 170 km/s, set A of parameters values, DM particle mass 16 GeV and $\xi\sigma_{SI}$ equal to 2.6·10^{-6} pb. *Right*: case of the C2 (Evans logarithmic) halo model with ρ_0 = 0.67 GeV/cm^3, v_0 = 170 km/s, set C of parameters values, DM particle mass 50 GeV and $\xi\sigma_{SI}$ equal to 1.2·10^{-6} pb. Obviously many other possibilities are open for good agreement including cases of the isothermal halo model usually used by other experiments in the field to report their results. (See color Figure on the journal website.)

In conclusion, the purely SI scenario is still supported by the data both for low and high mass candidates; the inclusion of the channeling effect also offers stringent agreement in many considered SI scenarios.

3.1.2. Candidates with isospin violating SI coupling

To study the case of a DM candidate with SI isospin violating interaction, where $f_p \neq f_n$, a third parameter, namely the ratio f_n/f_p, must be considered together with $\xi\sigma_{SI}$ and m_{DM}. Obviously the previous case of isospin conserving is restored whenever the ratio f_n/f_p = 1.

The results of the analysis are reported in Fig. 4, where the allowed regions in the f_n/f_p vs m_{DM} plane are shown after marginalizing on $\xi\sigma_{SI}$. For simplicity four halo models: A0 (isothermal sphere), B1, C1, D3 with the v_0 and ρ_0 in the range of Table III of Ref. [24], and three choices of the Na and I quenching factors: Q_I, Q_{II}, and including the channeling effect are considered.

Typically, a few considerations can be done:

- Two bands of m_{DM} can be recognized, as expected: one at low mass and the other at higher mass.

- The low mass DM candidates have a good fit in correspondence of $f_n/f_p \simeq -53/74 = -0.72$, where the ^{127}I contribution vanishes and the signal is mostly due to ^{23}Na recoils.

- Similarly, at larger mass $f_n/f_p \simeq -0.72$ is instead disfavored.

- The case of isospin-conserving f_n/f_p = 1 is well supported at different extent both at lower and larger mass.

- When the channeling effect is included (panels on the *right* of Fig. 4), the case of f_n/f_p = 1 at low mass has even stronger support, which is the higher confidence level. This argument is also supported by the agreement of the theoretical model and experimental data shown in Fig. 3 and in Fig. 5. In particular, in Fig. 5 the case of the isothermal sphere and v_0 = 220 km/s is considered.

- Contrary to what was stated in Ref. [58 - 60] where the low mass DM candidates were disfavored for f_n/f_p = 1 by DAMA data, the inclusion of the uncertainties related to halo models, v_0 and ρ_0, quenching factors, channeling effect, nuclear form factors, etc., and correctly accounting for other aspects, can also support low mass DM candidates either including or not the channeling effect. Some instances of this are reported in Figs. 2, 3, and 5.

In conclusion, at present level of uncertainties the DAMA data, if interpreted in terms of DM particle inducing nuclear recoils through SI interaction, can account either for low and large DM particle mass and for a wide range of the ratio f_n/f_p, even including the "standard" case f_n/f_p = 1.

3.1.3. Spin-Dependent interaction

The purely SD interaction, to which Na and I nuclei are fully sensitive, can also be considered. As mentioned above, any result and comparison, in this case, is even more uncertain considering the large uncertainties on spin factors and on form factor and the complementary sensitivities among different target nuclei depending on their unpaired nucleon [54, 15, 16].

The complete results would be described by a 3-dimensional volume: ($\xi\sigma_{SD}$, m_{DM}, θ). Thus, many possible configurations are available; here for simplicity, we show, as examples, the results obtained only for 4 particular couplings, which correspond to the following values of the mixing

angle θ: (i) θ = 0 ($a_n = 0$ and $a_p \neq 0$ or $|a_p| \gg |a_n|$); (ii) θ =π/4 ($a_p = a_n$); (iii) θ =π/2 ($a_n \neq 0$ and $a_p = 0$ or $|a_n| \gg |a_p|$); (iv) θ =2.435 rad ($a_n/a_p = -0.85$, pure Z_0 coupling). The case $a_p = -a_n$ is nearly similar to the case (iv).

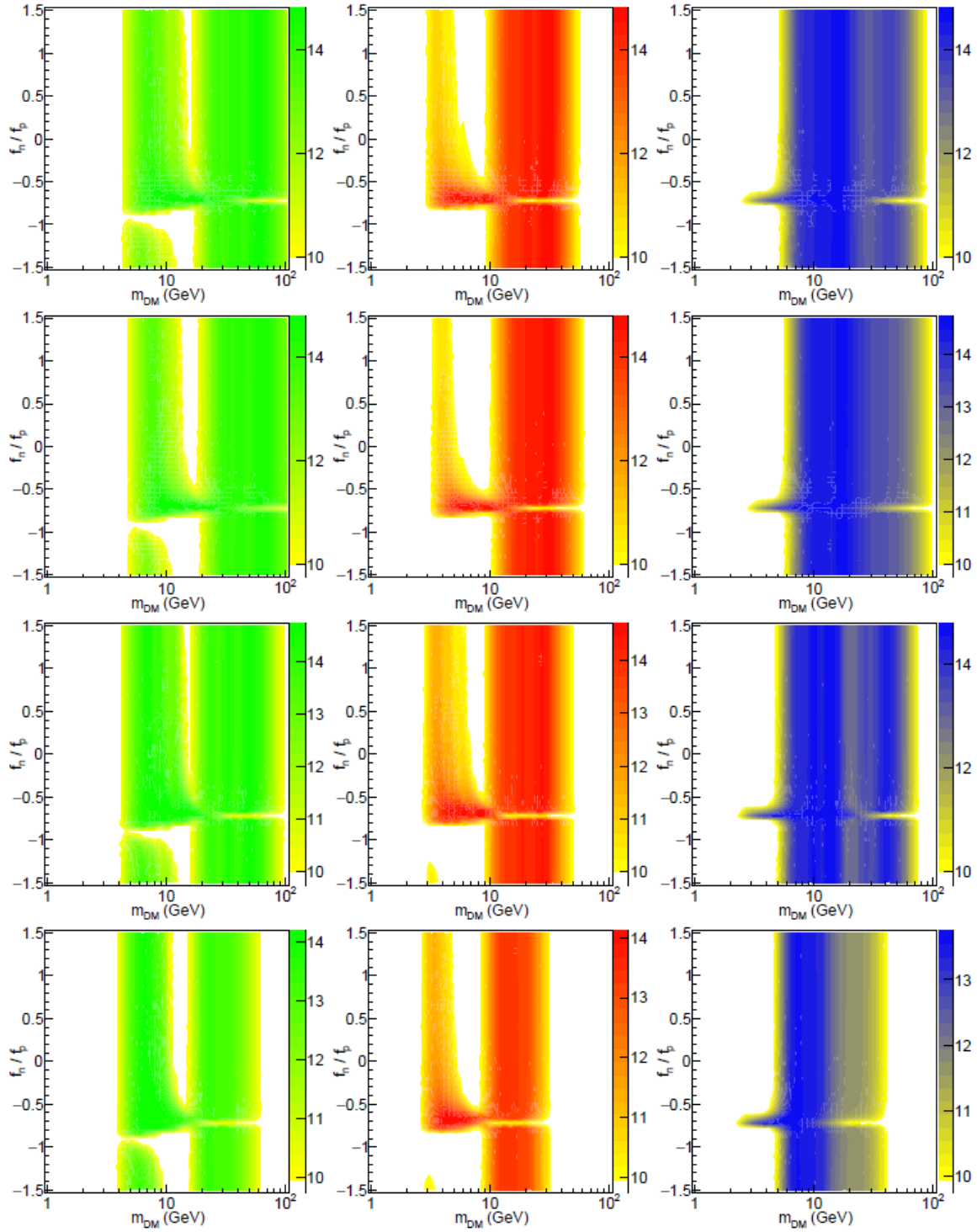

Fig. 4. Regions in the f_n/f_p vs m_{DM} plane allowed by DAMA experiments in the case of a Dark Matter candidate having isospin violating SI interaction. The Na and I quenching factors are: Q_I [*left* (green on-line)], Q_{II} [*center* (red on-line)], and with channeling effect [*right* (blue on-line)]. The considered halos (from top to bottom) are A0 (isothermal sphere), B1, C1, D3 with the v_0 and ρ_0 in the range of Table III of Ref. [24]. The three possible sets of parameters A, B and C are considered (see Sect. 2); the allowed regions represent the domain where the likelihood-function values differ more than 10 σ from the *null hypothesis* (absence of modulation). The color scales give the confidence level in units of σ from the *null hypothesis*. (See color Figure on the journal website.)

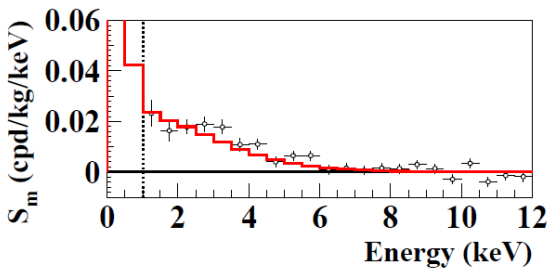

Fig. 5. Example of superposition of the measured S_m^{exp} vs energy (points with error bars) with theoretical expectations (solid histograms) for the SI case, when the channeling effect is included [28], for $m_{DM} = 11$ GeV and for the isothermal sphere halo model A0, with $v_0 = 220$ km/s and $\rho_0 = 0.3$ GeV/cm^3. The set A of parameter values and $\xi\sigma_{SI}$ equal to $7.0 \cdot 10^{-6}$ pb are taken into account.

In Fig. 6 slices ($\xi\sigma_{SD}$ vs m_{DM}) of the 3-dimensional allowed volume at the θ values are given above at 10 σ from the absence of signal are shown. For each configuration 3 regions are depicted accounting for the quenching factors uncertainties.

In Fig. 7 the experimental S_m values are compared with some of the expectations in this scenario. As can be seen, several configurations are in good agreement with the data. Obviously, much more can exist considering that only a few configurations of the 3-dimensional volume are depicted here.

Finally, Fig. 8 shows the allowed regions in the $\tan\theta$ vs m_{DM} plane after marginalizing on $\xi\sigma_{SD}$. For simplicity four halo models: A0 (isothermal sphere), B1, C1, D3 with the v_0 and ρ_0 in the range of Table III of Ref. [24], and three choices of the Na and I quenching factors: Q_I; Q_{II}, and including the channeling effect are considered.

In conclusion, the purely SD scenarios are in good agreement with the DAMA results and can explain the different capabilities of detection among targets with different unpaired nucleons. The large uncertainties e.g. in the spin factor also offer additional space for compatibility among different target nuclei.

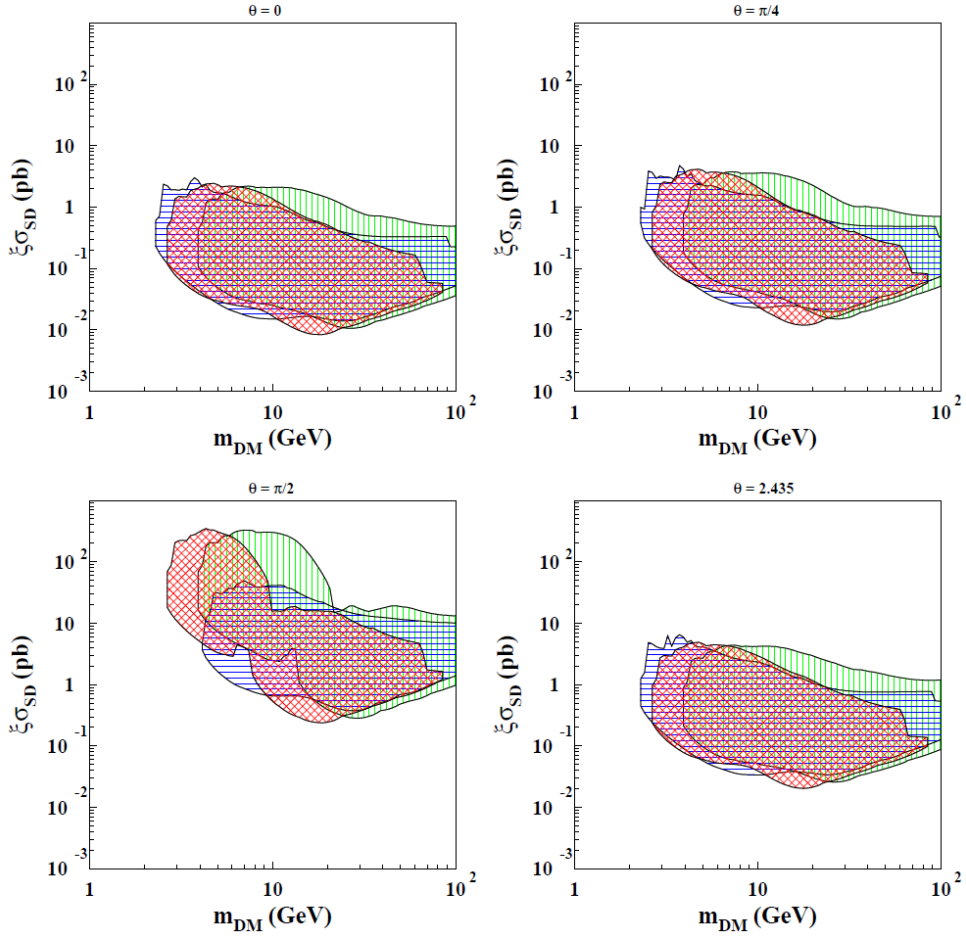

Fig. 6. Slices of the 3-dimensional volume ($\xi\sigma_{SD}$, m_{DM}, θ) allowed by DAMA experiments in the case of a Dark Matter candidate elastically scattering off target nuclei and SD interaction. Three different instances for the Na and I quenching factors have been considered: (i) Q_I case [(green on-line) vertically-hatched region], (ii) with channeling effect [(blue on-line) horizontally-hatched region] and (iii) Q_{II} [(red on-line) cross-hatched region]. The regions have been obtained by marginalizing all the models for each considered scenario (see Sect. 2) and they represent the domain where the likelihood-function values differ more than 10 σ from the *null hypothesis* (absence of modulation). (See color Figure on the journal website.)

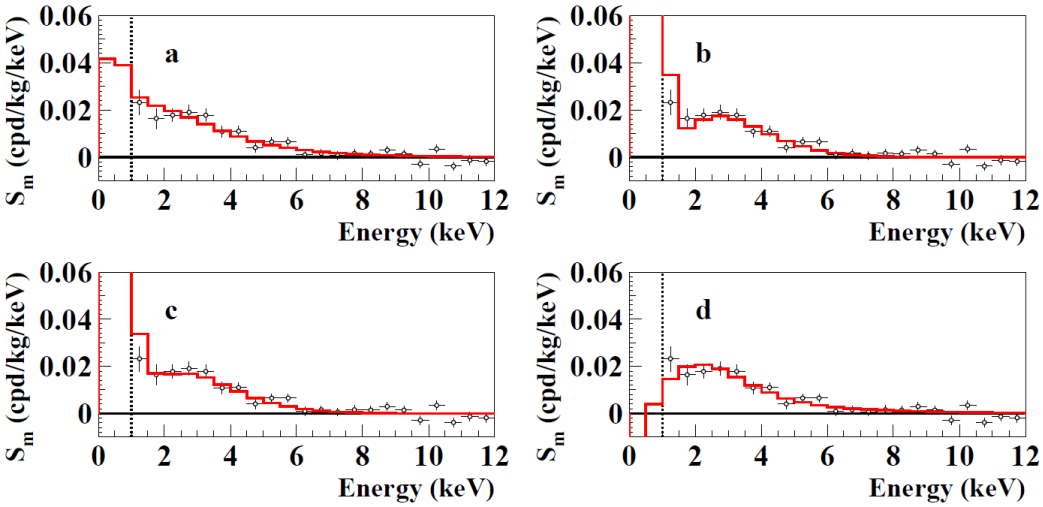

Fig. 7. Examples of superposition of the measured S_m^{exp} vs energy (points with error bars) with theoretical expectations (solid histograms) for the purely SD interaction. a – case of the A0 (isothermal sphere) halo model with $\rho_0 = 0.18$ GeV/cm^3, $v_0 = 170$ km/s, set B of parameters values, $\theta = 0$, $m_{DM} = 15$ GeV, $\xi\sigma_{SD} = 0.47$ pb including channeling effect; b – case of the C1 (Evans logarithmic) halo model with $\rho_0 = 0.94$ GeV/cm^3, $v_0 = 220$ km/s, set A of parameters values, $\theta = \pi/2$, $m_{DM} = 10$ GeV, $\xi\sigma_{SD} = 23$ pb and quenching Q_I; c – case of the C4 (Evans power-law) halo model with $\rho_0 = 0.65$ GeV/cm^3, $v_0 = 170$ km/s, set A of parameters values, $\theta = 2.435$, $m_{DM} = 8$ GeV, $\xi\sigma_{SD} = 0.49$ pb and quenching Q_{II}; d – case of the C2 (Evans logarithmic) halo model with $\rho_0 = 0.67$ GeV/cm^3, $v_0 = 170$ km/s, set C of parameters values, $\theta = \pi/4$, $m_{DM} = 52$ GeV, $\xi\sigma_{SD} = 0.10$ pb and quenching Q_I. (See color Figure on the journal website.)

3.1.4. Mixed coupling framework

The most general case is when both SI and SD couplings are considered. Details of related calculations can be found in Ref. [54, 15]. In this scenario, both the uncertainties on the SI and SD frameworks have to be accounted for. The complete result is given by a 4-dimensional allowed volume: ($\xi\sigma_{SI}$, $\xi\sigma_{SD}$, m_{DM}, θ). The isospin violating SI interaction is not included hereafter.

For simplicity examples of slices ($\xi\sigma_{SI}$, $\xi\sigma_{SD}$) at 10 σ from the *null hypothesis* (absence of modulation) are shown in Fig. 9 for some choices of m_{DM} and θ values.

Obviously, the proper accounting for the complete 4-dimensional allowed volume and the existing uncertainties and complementarity largely extend the results and any comparison.

Finally, let us now point out that configurations with $\xi\sigma_{SI}$ ($\xi\sigma_{SD}$) even much lower than those shown in Fig. 1 (Fig. 6) would be possible if a small SD (SI) contribution would be present in the interaction. This possibility is clearly pointed out in Figs. 10 and 11 where some examples of regions in the plane cross-section vs m_{DM} are reported. As it can be seen, these arguments clearly show that even a relatively small SD (SI) contribution can drastically change the allowed region in the (m_{DM}, $\xi\sigma_{SI(SD)}$) plane; therefore, the typically shown model-dependent comparison plots between exclusion limits at a given C.L. and regions of allowed parameter space do not hold e.g. for mixed scenarios when comparing experiments with and without sensitivity to the SD component of the interaction. The same happens when comparing regions allowed by experiments whose target-nuclei have unpaired proton with exclusion plots quoted by experiments using target-nuclei with unpaired neutron when the SD component of the interaction would correspond either to $\theta \simeq 0$ or $\theta \simeq \pi$.

3.2. DM particles with preferred electron interaction

Some extensions of the standard model provide DM candidate particles, which can have a dominant coupling with the lepton sector of the ordinary matter. Thus, such DM candidate particles can be directly detected only through their interaction with electrons in the detectors of a suitable experiment, while they cannot be studied in those experimental results where subtraction/rejection of the electromagnetic component of the experimental counting rate is applied[12]. These candidates can also offer a possible source of the 511 keV photons observed from the galactic bulge. This scenario was already investigated by DAMA with lower exposure [29].

[12] If the electron is assumed at rest, considering the DM particle velocity, the released energy would be of order of few eV, well below the detectable energy in any considered detector in the field. However, the electron is bound in the atom and, even if the atom is at rest, the electron can have non-negligible momentum, as shown in Ref. [29].

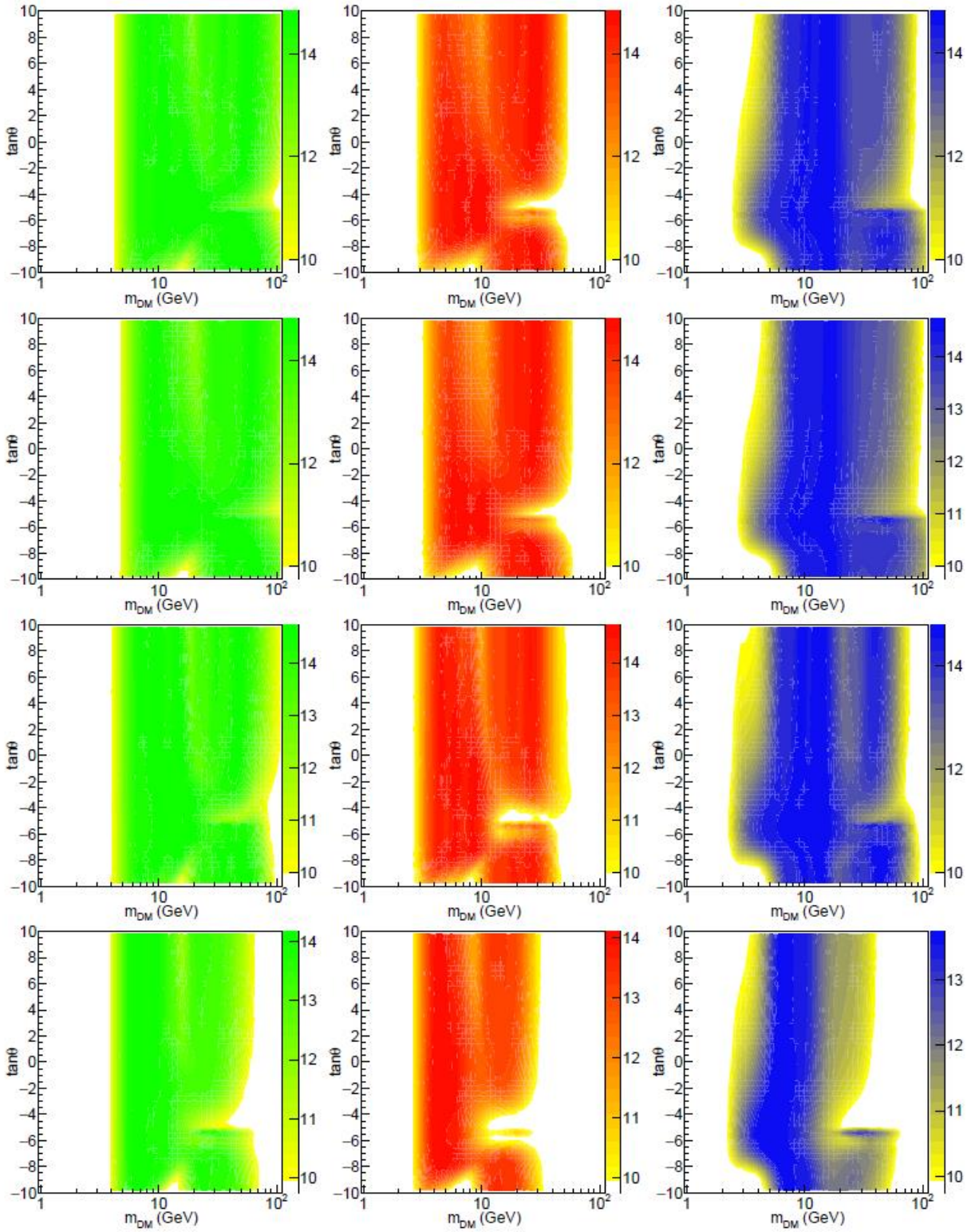

Fig. 8. Regions in the tanθ vs m_{DM} plane allowed by DAMA experiments in the case of a DM candidate with SD interaction. The Na and I quenching factors are: Q_I [*left* (green on-line)], Q_{II} [*center* (red on-line)], and with channeling effect [*right* (blue on-line)]. The considered halos (from top to bottom) are A0 (isothermal sphere), B1, C1, D3 with the v_0 and ρ_0 in the range of Table III of Ref. [24]. The three possible sets of parameters A, B and C are considered (see Sect. 2); the allowed regions represent the domain where the likelihood-function values differ more than 10 σ from the *null hypothesis* (absence of modulation). The color scales give the confidence level in units of σ from the *null hypothesis*. (See color Figure on the journal website.)

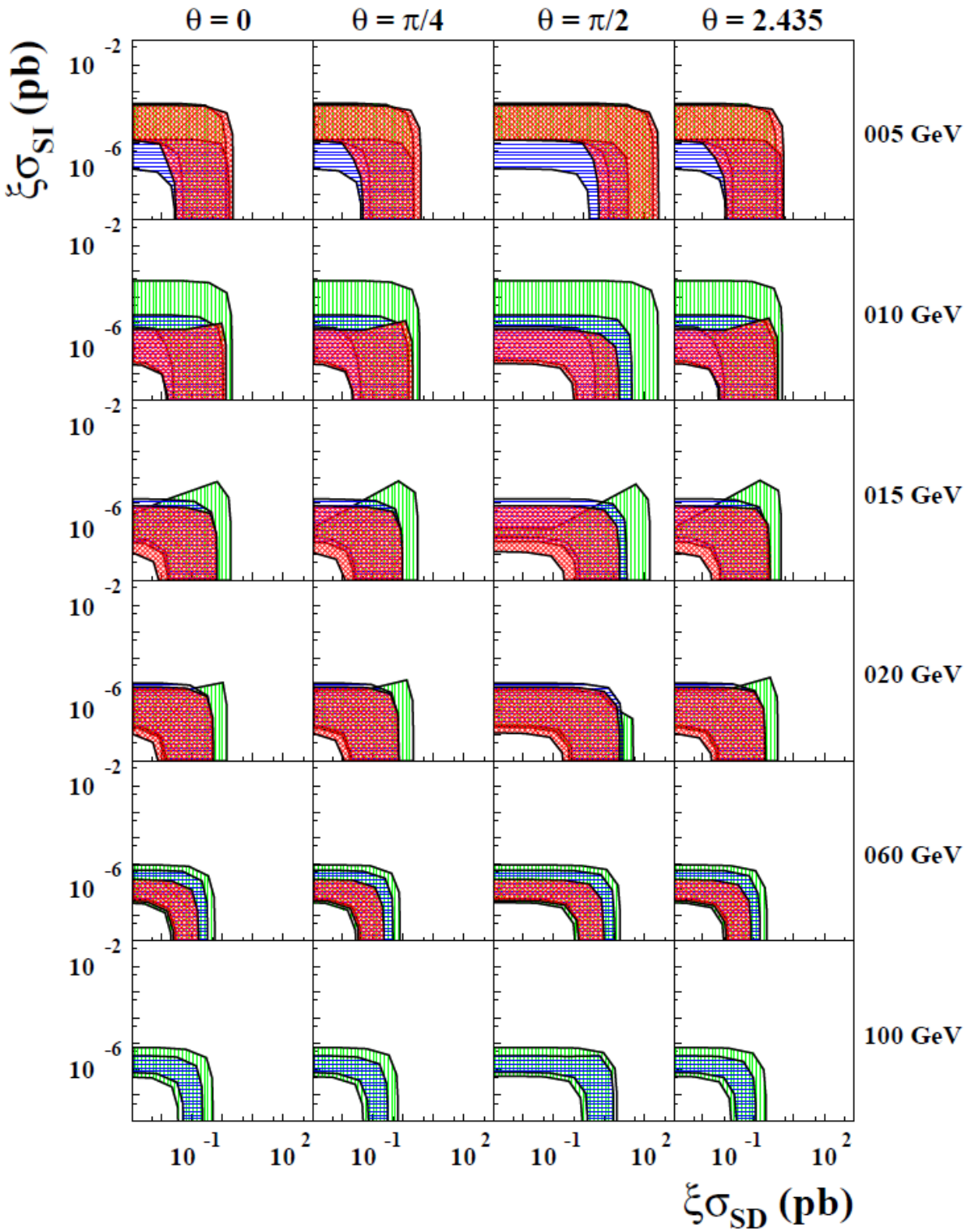

Fig. 9. Slices of the 4-dimensional volume ($\xi\sigma_{SI}$, $\xi\sigma_{SD}$, m_{DM}, θ) allowed by all DAMA experiments in the case of a DM candidate with elastic scattering off target nuclei and mixed SI and SD interaction. Three different instances for the Na and I quenching factors have been considered: (i) Q_I case [(green on-line) vertically-hatched region], (ii) with channeling effect [(blue on-line) horizontally-hatched region] and (iii) Q_{II} [(red on-line) cross-hatched region]. The regions have been obtained by marginalizing all the models for each considered scenario (see Sect. 2) and they represent the domain where the likelihood-function values differ more than 10 σ from the *null hypothesis* (absence of modulation). (See color Figure on the journal website.)

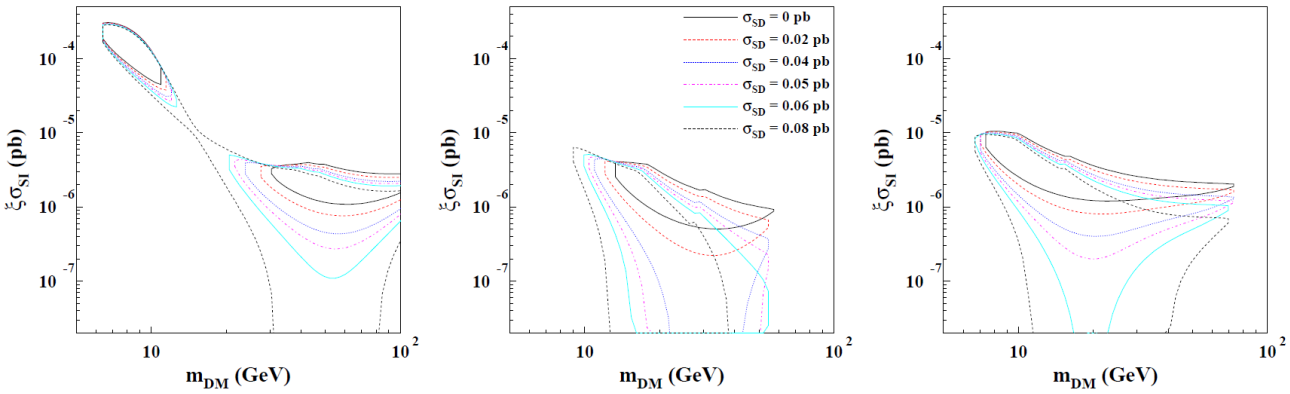

Fig. 10. An example of the effect induced by the inclusion of a SD component different from zero on allowed regions given in the plane $\xi\sigma_{SI}$ vs m_{DM}. In this example the B1 halo model with v_0 = 170 km/s and ρ_0 = 0.42 GeV/cm^3, the set of parameters A and the particular case of θ = 0 for the SD interaction have been considered. The used quenching factors are Q_I (*left*), Q_{II} (*center*) and channeling effect (*right*). From top to bottom the contours refer to different SD contributions: σ_{SD} = 0 pb (solid black line), 0.02 pb, 0.04 pb, 0.05 pb, 0.06 pb and 0.08 pb. Analogous situation is found for the other model frameworks. (See color Figure on the journal website.)

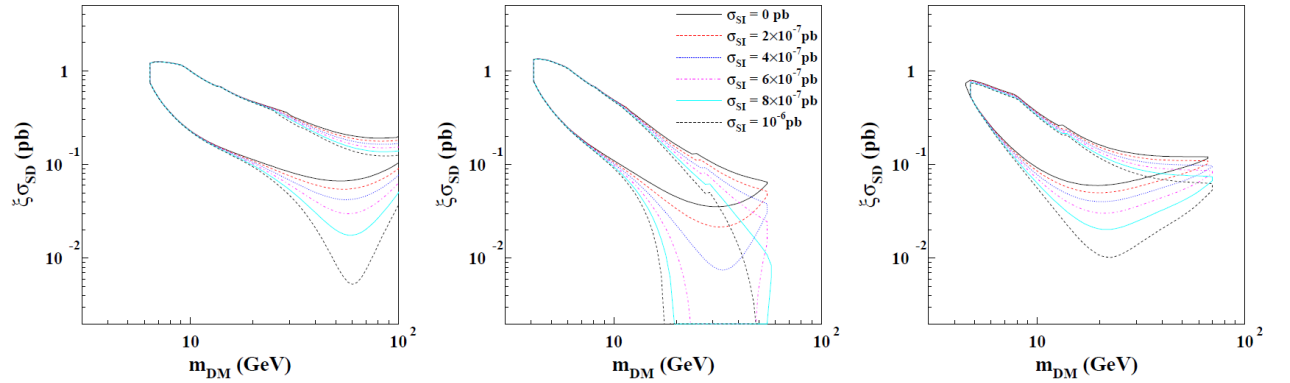

Fig. 11. An example of the effect induced by the inclusion of a SI component different from zero on allowed regions given in the plane $\xi\sigma_{SD}$ vs m_{DM}. The same halo model, parameter set and θ value of Fig. 10 have been considered. The used quenching factors are Q_I (*left*), Q_{II} (*center*) and channeling effect (*right*). From top to bottom the contours refer to different SI contributions: σ_{SI} = 0 pb (solid black line), 2·10^{-7} pb, 4·10^{-7} pb, 6·10^{-7} pb, 8· 10^{-7} pb, 10^{-6} pb. The analogous situation is found for other model frameworks. (See color Figure on the journal website.)

In particular, as shown in Ref. [29], such DM candidate particles with mass $\gtrsim$ few GeV can interact on bound electrons with momentum up to $\simeq$ few MeV/c; thus, they can provide signals in the keV energy region detectable by low background and low energy threshold detectors, such as those of DAMA. The expected differential energy spectrum has been derived in Ref. [29]; it depends on a single parameter, $\xi\sigma_e^0/m_{DM}$, for each halo model. Here, σ_e^0 is the DM particle cross-section on the electron at rest [29].

With the new cumulative exposure, we have derived the results following the same procedure as in Ref. [29], and the prescription of Sect. 2. The expected behaviour of the modulation amplitudes rapidly rises at low energy [29]; an example is also reported in Fig. 12. On the contrary, the measured modulation amplitudes have a smooth trend with energy even below 2 keV. In particular, this has been pointed out by the new results of

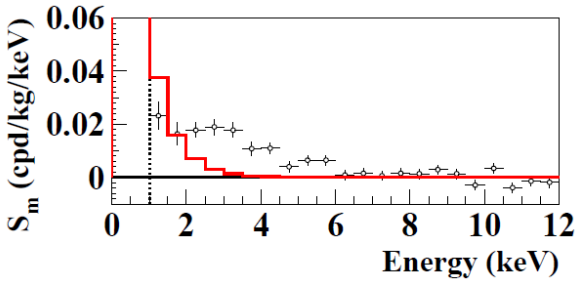

Fig. 12. Example of superposition of the measured S_m^{exp} vs energy (points with error bars) with theoretical expectations (solid histograms) for DM particles with preferred electron interaction. The case of the C2 (Evans logarithmic) corotating halo model with ρ_0 = = 0.67 GeV/cm^3, v_0 = 170 km/s and $\xi\sigma_e^0/m_{DM}$ = = 9.5·10^{-4} pb/GeV is considered. This is an example of how to disentangle among some scenarios, improving the sensitivity of the set-up. (See color Figure on the journal website.)

DAMA/LIBRA-phase2. Thus, the lower energy threshold achieved by DAMA/LIBRA-phase2 at 1 keV prevents finding configurations for these DM candidates *distant* more than 10 σ from the *null hypothesis*. This is an example of how to disentangle among some scenarios, improving the sensitivity of the set-up.

However, just for these DM candidates, we can apply a less severe confidence level. Thus, Fig. 13 shows the allowed region in the ($\xi\sigma_e^0$ vs m_{DM}) plane for the dark halo models and related parameters described above. The region encloses configurations *distant* more than 8 σ from the *null hypothesis*. At such a confidence level about half dark halo, models provide allowed interval for the $\xi\sigma_e^0/m_{DM}$ parameter. We note that, although the mass region in the plot is up to 2 TeV, m_{DM} particles with larger masses are also allowed.

The results are given here hold for every kind of DM candidate interacting with electrons and with cross-section σ_e having a weak dependence on electron momentum and DM particle velocity [29].

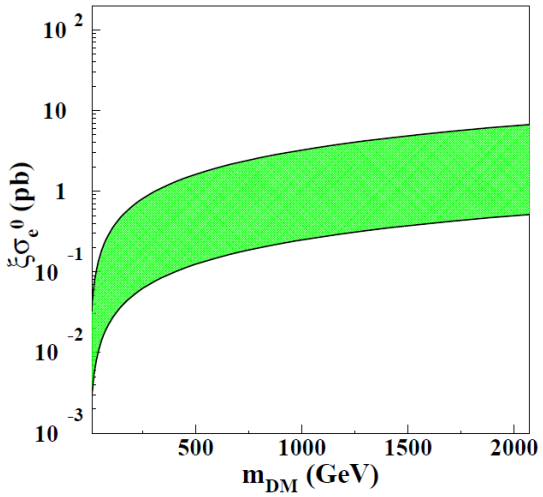

Fig. 13. Region allowed in the ($\xi\sigma_e^0$ vs m_{DM}) plane for the same dark halo models and related parameters described above. The region encloses configurations *distant* more than 8 σ from the *null hypothesis*. The C.L. suggests that this kind of scenario is less favored by the data with respect to other ones considered in this paper. We note that, although the mass region in the plot is up to 2 TeV, m_{DM} particles with larger masses are also allowed. (See color Figure on the journal website.)

There U boson with M_U masses in the sub-GeV range (see Ref. [29] for details) is well allowed for a large interval of m_{DM}.

In conclusion, the obtained allowed interval for the mass of the possible mediator of the interaction is well in agreement with the typical requirements of the phenomenological analyses available in the literature.

The hypothesis of a 4-fermion point contact interaction can be described by a possible mediator of the interaction (hereafter U boson) with mass M_U larger than the transferred momentum ($M_U \gtrsim$ $\gtrsim 10$ MeV). In the pure $V \pm A$ and pure scalar scenario, the effective coupling constant, G, depends on the couplings, c_e, and c_{DM}, of the U boson with the electron and the DM particle, respectively. The cross-section on the electron at rest is:

$$\sigma_e^0 = \frac{c_e^2 c_{DM}^2 m_e^2}{\pi M_U^4}.$$

Following the procedure of Ref. [29], that considers: i) the limit on c_e from $g_e - 2$ data; ii) $c_{DM} <$ $< \sqrt{4\pi}$, that is the theory is perturbative; iii) the obtained lower bound $\xi\sigma_e^0/m_{DM} > 2.5\cdot10^{-4}$ pb/GeV from the cumulative 2.46 t· yr data set (as shown in Fig. 13); iv) $\xi \leq 1$; the allowed U boson masses are: $M_U(\text{GeV}) \lesssim \sqrt{16285/m_{DM}(\text{GeV})}$, for configurations *distant* more than 8 σ from the *null hypothesis*. They are reported in Fig. 14.

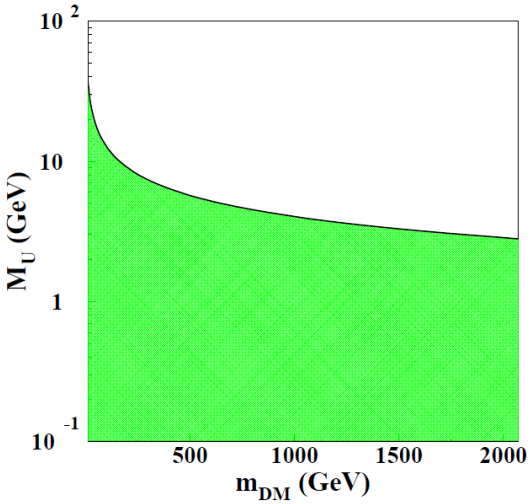

Fig. 14. Region of U boson mass allowed by present analysis considering [29]: i) the limit on c_e from $g_e - 2$ data; ii) $c_{DM} < \sqrt{4\pi}$, that is the theory is perturbative; iii) the obtained lower bound $\xi\sigma_e^0/m_{DM} > 2.5\cdot10^{-4}$ pb/GeV from the new cumulative data set (as shown in Fig. 13); iv) $\xi \leq 1$. U boson with M_U masses in the sub-GeV range is well allowed for a large interval of m_{DM}. (See color Figure on the journal website.)

3.3. Inelastic Dark Matter

Another scenario that will be updated here regards the inelastic Dark Matter: relic particles that cannot scatter elastically off nuclei. Following an inelastic scattering of a nucleus, the kinetic energy of the recoiling nucleus is quenched and is the detected quantity. As discussed in Refs. [61 - 63, 23], the

inelastic Dark Matter could arise from a massive complex scalar split into two approximately degenerate real scalars or from a Dirac fermion split into two approximately degenerate Majorana fermions, namely χ_+ and χ_-, with a δ mass splitting. In particular, a specific model featuring a real component of the sneutrino, in which the mass splitting naturally arises, has been given in Ref. [61].

The discussion of the theoretical arguments on such inelastic Dark Matter can be found e.g. in Ref. [61], where it was shown that for the χ_- inelastic scattering off target nuclei a kinematic constraint exists which favors heavy nuclei (such as ^{127}I) with respect to lighter ones (such as e.g. ^{nat}Ge) as target-detectors media. In fact, χ_- can only inelastically scatter by transitioning to χ_+ (slightly heavier state than χ_-) and this process can occur only if the χ_- velocity, v, is larger than:

$$v_{thr} = \sqrt{\frac{2\delta}{m_{red}(A,\chi)}}, \qquad (6)$$

where $m_{red}(A,\chi)$ is the χ – nucleus reduced mass. This kinematic constraint becomes increasingly severe as the nucleus mass, m_N, is decreased [61]. For example, if $\delta \geq 100$ keV, a signal rate measured e.g. in Iodine will be a factor about 10 or higher than that measured in Ge [61]. Moreover, this model scenario implies some characteristic features when exploiting the DM annual modulation signature since it gives rise to an enhanced modulated component, S_m, with respect to the un-modulated one, S_0, and to largely different behaviors with energy for both S_0 and S_m (both show a higher mean value) [61] with respect to elastic cases. Details of calculation procedures can be found in Ref. [23].

Accounting for the uncertainties mentioned above, in the inelastic Dark Matter scenario, an allowed 3-dimensional volume in the space ($\xi\sigma_p$, m_{DM}, δ) is obtained. Here, following the notation of Ref. [23], σ_p is a generalized SI point-like χ-nucleon cross-section and m_{DM} is the χ mass.

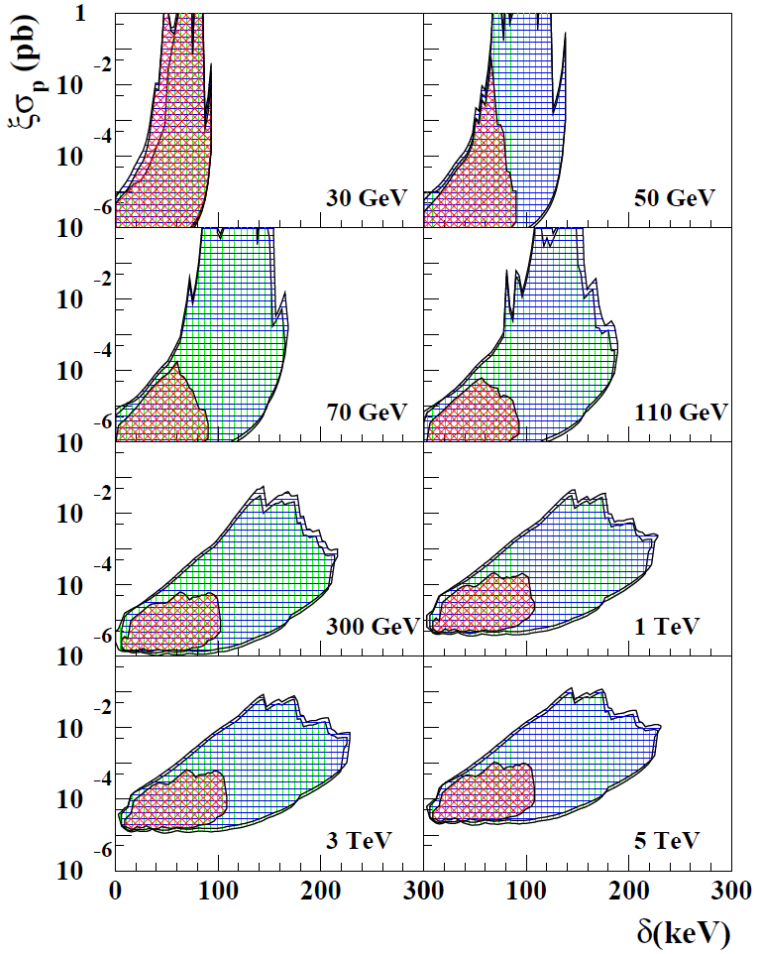

Fig. 15. Slices of the 3-dimensional volume ($\xi\sigma_p$, δ, m_{DM}) allowed by DAMA experiments in the case of a Dark Matter candidate with preferred inelastic interaction. Three different instances for the Na and I quenching factors have been considered: (i) Q_I case [(green on-line) vertically-hatched region], (ii) with channeling effect [(blue on-line) horizontally-hatched region] and (iii) Q_{II} [(red on-line) cross-hatched region]. The regions have been obtained by marginalizing all the models for each considered scenario (see Sect. 2) and they represent the domain where the likelihood-function values differ more than 10 σ from the *null hypothesis* (absence of modulation). (See color Figure on the journal website.)

For simplicity, Fig. 15 shows slices of such an allowed volume at 10 σ from the *null hypothesis* for some values of m_{DM}; the different cases of quenching factors are considered as well. It can be noted that when $m_{DM} \gg m_N$, the expected differential energy spectrum is trivially dependent on m_{DM} and, in particular, it is proportional to the ratio between $\xi\sigma_p$ and m_{DM}. Thus, allowed regions for other $m_{DM} \gg m_N$ can be obtained from the last panel of Fig. 15, straightforward.

Significant enlargement of such regions should be expected when including the complete effects of model (and related experimental and theoretical parameters) uncertainties.

In Fig. 16 few examples of comparison between S_m^{exp} and S_m^{th} are shown.

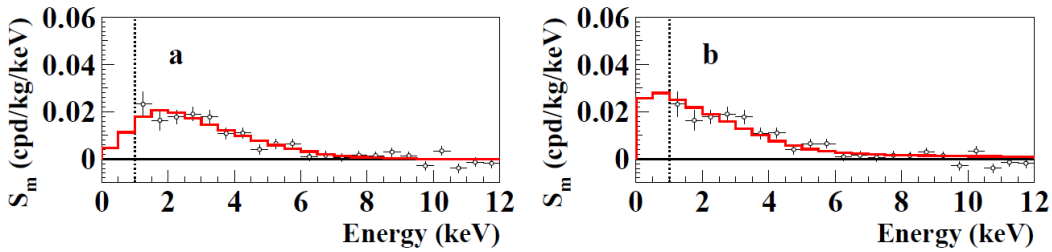

Fig. 16. Examples of superposition of the measured S_m^{exp} vs energy (points with error bars) with theoretical expectations (solid histograms) for Inelastic Dark Matter. a – case of the B2 (Evans power-law) halo model with ρ_0 = 1.33 GeV/cm^3, v_0 = 270 km/s, set B of parameters values, m_{DM} = 50 GeV, δ = 75 keV, $\xi\sigma_p = 1.1\cdot10^{-6}$ pb and quenching Q_I; b – case of the B4 (Jaffe) halo model with ρ_0 = 0.44 GeV/cm^3, v_0 = 220 km/s, set C of parameters values, m_{DM} = 30 GeV, δ = 25 keV, $\xi\sigma_p = 4.2\cdot10^{-6}$ pb including channeling effect. (See color Figure on the journal website.)

Finally, Fig. 17 shows the allowed regions in the δ vs m_{DM} plane after marginalizing on $\xi\sigma_p$. For simplicity four halo models: A0 (isothermal sphere), B1, C1, D3 with the v_0 and ρ_0 in the range of Table III of Ref. [24], and three choices of the Na and I quenching factors: Q_I, Q_{II}, and including the channeling effect are considered.

Let us conclude that here the analysis of the inelastic DM particle has been limited only to SI coupling. Recently analyses of the inelastic DM candidate with SD coupling have been reported in Refs. [64, 65]. They show that also this scenario can be compatible with the DAMA result. This conclusion can be further confirmed considering e.g. the effects of uncertainties in the models that in those papers have not been included.

3.3.1. Including the Thallium

Until now, we have considered the NaI(Tl) detectors made of Sodium and Iodine nuclei; however, the Thallium dopant (stable isotopes with mass number 203 and 205, and natural abundances 29.5 and 70.5 %, respectively) can also play a role as it has been described in Ref. [66], where it has been shown how the DM interaction on Thallium nuclei would give rise to a signal which cannot be detected with lower mass target-nuclei. This also can decouple theoretical and experimental aspects from different experiments. The slices of the 3-dimensional volume ($\xi\sigma_p$, δ, m_{DM}), allowed by DAMA experiments when the inelastic scattering off Thallium nuclei is also included, have been evaluated in Fig. 18 for some examples of scenarios, and in Fig. 19 marginalizing all the considered models (see Sect. 2). Two instances for the Tl quenching factor in NaI(Tl) are considered: (i) Q_I case with q_{Tl} = 0.075, tentatively obtained by extrapolating the q_{Na} and q_I measured by DAMA with neutrons [49]; (ii) Q_{II} quenching factors varying as a function of E_R evaluated as in Ref. [50]. Moreover, the Thallium is assumed to be homogeneously distributed in each crystal and among the crystals at the level of 0.1 % in mass (corresponding to $2.95\cdot10^{21}$ Tl atoms/kg).

Thus, we have verified that, as pointed out in Figs. 18 and 19, new regions with $\xi\sigma_p \gtrsim 1$ pb and $\delta \gtrsim 100$ keV are allowed by DAMA after the inclusion of the inelastic scattering off Thallium nuclei. Such regions are not fully accessible to detectors with target nuclei having mass lower than Thallium.

In Fig. 20 two examples of comparison between S_m^{exp} and S_m^{th} are shown; both the configurations belong to the additional allowed regions obtained when taking into account the presence of the Thallium nuclide in the NaI(Tl) detectors (see Figs. 18 and 19).

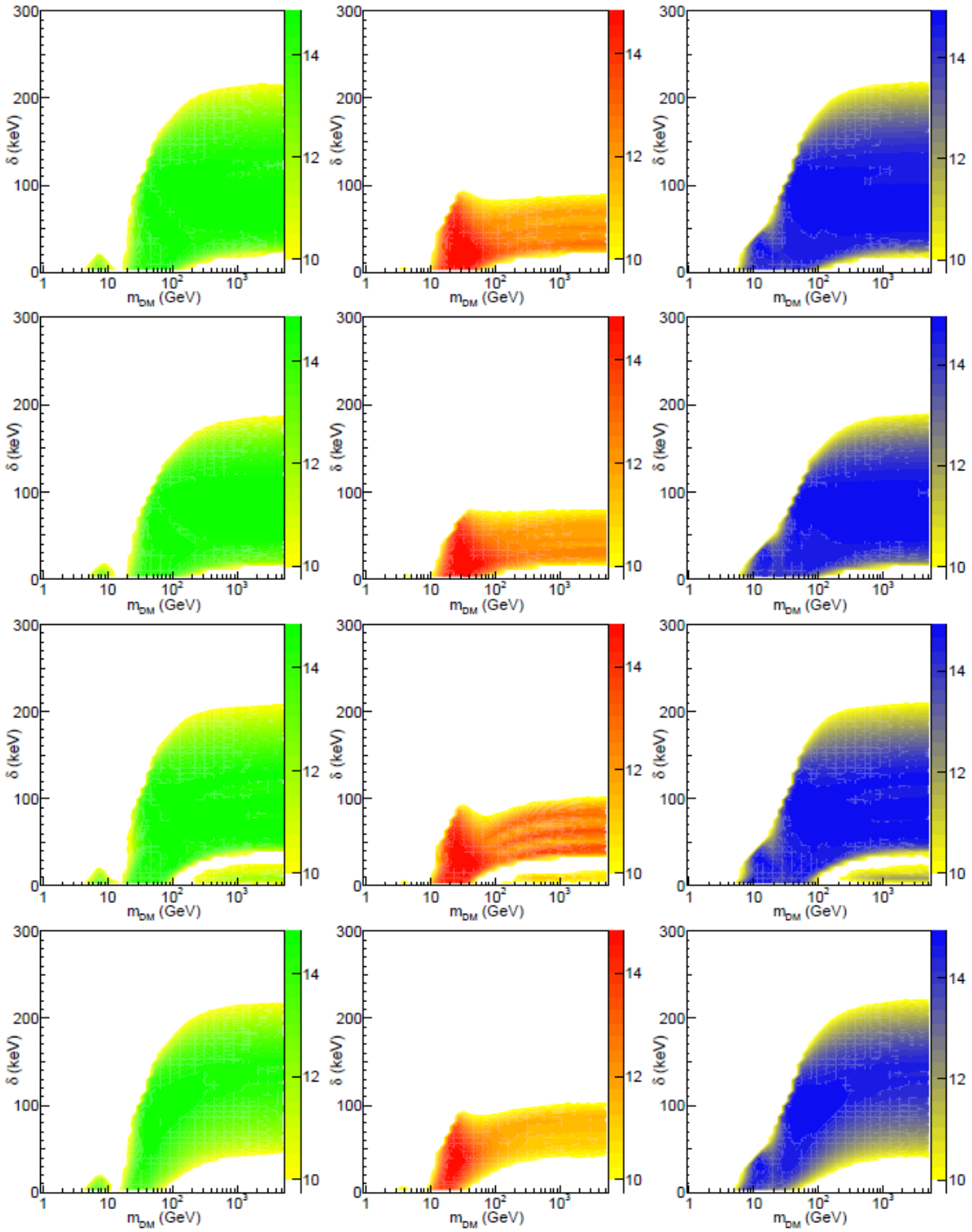

Fig. 17. Regions in the δ vs m_{DM} plane allowed by DAMA experiments in the case of a Dark Matter candidate with preferred inelastic interaction. The Na and I quenching factors are: Q_I [*left* (green on-line)], Q_{II} [*center* (red on-line)], and with channeling effect [*right* (blue on-line)]. The considered halos (from top to bottom) are A0 (isothermal sphere), B1, C1, D3 with the v_0 and ρ_0 in the range of Table III of Ref. [24]. The three possible sets of parameters A, B and C are considered (see Sect. 2); the allowed regions represent the domain where the likelihood-function values differ more than 10 σ from the *null hypothesis* (absence of modulation). The color scales give the confidence level in units of σ from the *null hypothesis*. (See color Figure on the journal website.)

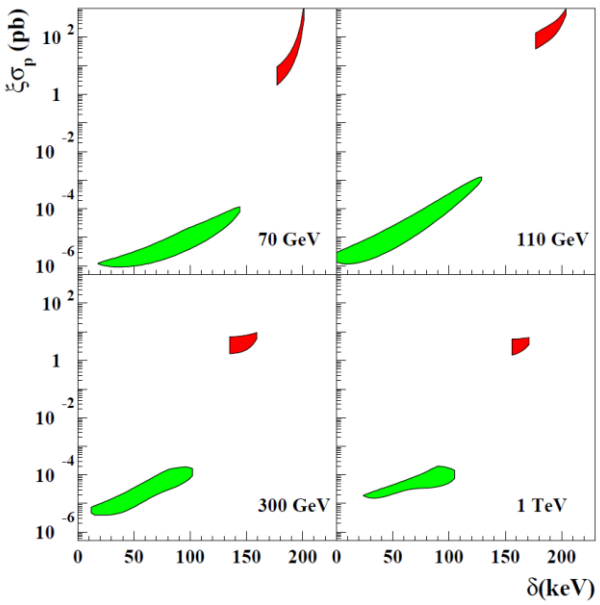

Fig. 18. Slices of the 3-dimensional volume ($\xi\sigma_p$, δ, m_{DM}) allowed by DAMA experiments for some example of scenarios when inelastic scattering only off Na and I nuclei is considered (green on-line region) and when the Thallium nuclei are also included (additional red on-line region). The four examples have been obtained considering the quenching case Q_I, the set C of parameter values and four different DM mass and halo models. In particular: the A3 (Evans power-law) halo model with $\rho_0 = 0.52$ GeV/cm^3 and $v_0 = 270$ km/s for $m_{DM} = 70$ GeV, the D4 (Triaxial) halo model with $\rho_0 = 0.30$ GeV/cm^3 and $v_0 = 170$ km/s for $m_{DM} = 110$ GeV, the B1 (Evans logarithmic) halo model with $\rho_0 = 0.20$ GeV/cm^3 and $v_0 = 170$ km/s for $m_{DM} = 300$ GeV and the B4 (Jaffe) halo model with $\rho_0 = 0.26$ GeV/cm^3 and $v_0 = 170$ km/s for $m_{DM} = 1$ TeV. The regions represent the domain where the likelihood-function values differ more than 10 σ from the *null hypothesis* (absence of modulation). (See color Figure on the journal website.)

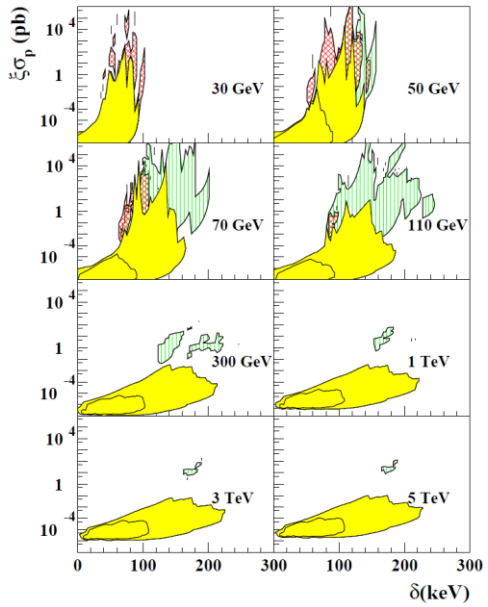

Fig. 19. Slices of the 3-dimensional volume ($\xi\sigma_p$, δ, m_{DM}) allowed by DAMA experiments when the inelastic scattering off Thallium nuclei is also included. The two instances for the Na, I, and Tl quenching factors are considered: (i) Q_I case [(green on-line) vertically-hatched region], (ii) Q_{II} [(red on-line) cross-hatched region]. The regions due to inelastic scattering only off Na and I nuclei, already shown in Fig. 15, are reported in (yellow on-line) light-filled. The regions have been obtained by marginalizing all the models for each considered scenario (see Sect. 2) and they represent the domain where the likelihood-function values differ more than 10 σ from the *null hypothesis* (absence of modulation). (See color Figure on the journal website.)

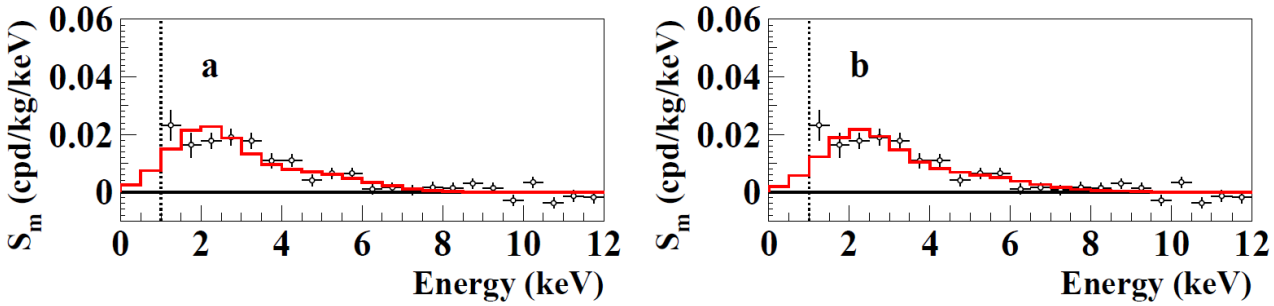

Fig. 20. Examples of superposition of the measured S_m^{exp} vs energy (points with error bars) with theoretical expectations (solid histograms) for Inelastic Dark Matter when including the Thallium nuclide. a – case of the A4 (Jaffe) halo model with $\rho_0 = 0.44$ GeV/cm^3, $v_0 = 220$ km/s, set A of parameters values, $m_{DM} = 70$ GeV, $\delta = 147$ keV, $\xi\sigma_p = 23$ pb and quenching Q_I; b – case of the A7 (Kravtsov et al.) halo model with $\rho_0 = 0.32$ GeV/cm^3, $v_0 = 170$ km/s, set A of parameters values, $m_{DM} = 110$ GeV, $\delta = 126$ keV, $\xi\sigma_p = 40$ pb and quenching Q_I. Both the configurations belong to the additional allowed regions obtained when taking into account the presence of the Thallium nuclide in the NaI(Tl) detectors (see Figs. 18 and 19). (See color Figure on the journal website.)

3.4. Investigation on light dark matter

Some extensions of the Standard Model provide DM candidate particles with sub-GeV mass; in the following, these candidates will be indicated as Light Dark Matter (LDM).

Several LDM candidates have been proposed in Warm Dark Matter scenarios, as the keV-scale sterile neutrino, axino, gravitino, and MeV-scale particles (for details see Ref. [30]).

In this section the direct detection of LDM candidate particles is investigated considering the possible inelastic scattering channels either off the electrons or off the nuclei of the target; theoretical expectations are compared with the recent results obtained by adding DAMA/LIBRA-phase2 [3 - 7]. Firstly we note that – since the kinetic energy for LDM particles in the galactic halo does not exceed hundreds eV – the elastic scattering of such LDM particles both off electrons and off nuclei yields energy releases hardly detectable by the detectors used in the field; this might prevent the exploitation of the elastic scattering as detection approach for these candidates. Thus, the inelastic process could be the only possible viable one for the direct detection of LDM; further details were given in Ref. [30].

The following process is, therefore, considered for detection: the LDM candidate (hereafter named ν_H with mass m_H) interacts with the ordinary matter target, T, with mass m_T. The target T can be either an atomic nucleus or an atomic electron depending on the nature of the ν_H particle interaction. As a result of the interaction, a lighter particle is produced (hereafter ν_L with mass $m_L < m_H$) and the target recoils with an energy E_R, which can be detectable by suitable detectors.

The lighter particle ν_L is neutral and it is required that it interacts very weakly with ordinary matter or not at all; thus, the ν_L particle escapes the detector. In particular, the ν_L particle can also be another DM halo component (dominant or sub-dominant with respect to the ν_H one), or it can simply be a Standard Model particle (e.g. ν_L can be identified with an active neutrino). Details can be found in Ref. [30].

Since the sub-GeV LDM wavelength ($\lambda = h/k > 10^3$ fm) is much larger than the nucleus size, the targets can be considered as point-like and the form factors of the targets can be approximated by one. The cross-section of the processes, σ_T, is generally a function of the LDM velocity, v, and can be written by adopting the approximation for the non-relativistic case [30]:

$$\sigma_T v \simeq a + bv^2, \qquad (7)$$

where a and b are constants depending on the peculiarity of the particle interaction with the target T. In the analysis, the cross-sections $\sigma_0^T = a / v_0$ and $\sigma_m^T = bv_0$ are defined [30]; they are related to the a and b parameters rescaled with the DM local velocity, v_0. In particular, the σ_m^T is responsible for the annual modulation of the expected counting rate for LDM interactions, and in the following, it will be used as a free parameter, together with m_H and the mass splitting $\Delta = m_H - m_L$. Moreover, for the case of LDM interaction on nuclei, following the prescriptions given in Ref. [30], two different nuclear-scaling laws are adopted: the coherent ($\sigma_m^{coh} \propto \sigma_m^{Na} / A_{Na}^2 \propto \sigma_m^I / A_I^2$) and the incoherent ($\sigma_m^{inc} \propto \sigma_m^{Na} \propto \sigma_m^I$) ones.

3.4.1. Interaction with atomic electrons

After the interaction of ν_H with an electron in the detector, the final state can have – beyond the ν_L particle – either a prompt electron and an ionized atom or an excited atom plus possible X-rays/Auger electrons. Therefore, the process produces X-rays and electrons of relatively low energy, which are mostly contained with efficiency $\simeq 1$ in a detector of a suitable size.

Comparing the expected modulated signal for this scenario with the experimental result obtained cumulatively by DAMA/NaI, DAMA/LIBRA-phase1 and DAMA/LIBRA-phase2 [3 - 7], it is possible to determine a $10\,\sigma$ C.L. allowed volume in the space (m_H, Δ, $\xi\sigma_m^e$). The projection of such a region on the plane (m_H, Δ) for the dark halo models and parameters described before is reported in Fig. 21.

The allowed m_H values and the splitting Δ are in the intervals 40 keV $\lesssim m_H \lesssim$ O(GeV) [13] and 1.5 keV $\lesssim \Delta \lesssim$ 70 keV, respectively. It is worth noting that in such a case the decay through the detection channel: $\nu_H \to \nu_L e^+ e^-$, is energetically forbidden for the given Δ range. The configurations with $m_H \gtrsim 511$ keV (dark area in Fig. 21) are instead of interest for the possible annihilation processes: $\nu_H \bar{\nu}_H \to e^+ e^-$, $\nu_H \bar{\nu}_L \to e^+ e^-$, $\nu_L \bar{\nu}_H \to e^+ e^-$, and $\nu_L \bar{\nu}_L \to e^+ e^-$, in the galactic center.

As examples, some slices of the 3-dimensional allowed volume for various m_H values in the ($\xi\sigma_m^e$ vs Δ) plane are depicted in Fig. 22, *left*.

[13] For values of m_H greater than O(GeV), the definition of LDM is no longer appropriate. Moreover, the kinetic energy of the particle would be enough for the detection in DAMA experiments also through the elastic scattering process, as demonstrated in Ref. [29].

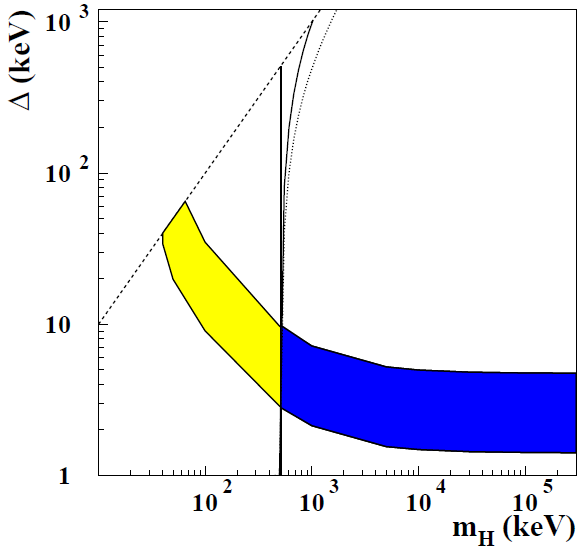

Fig. 21. Projection of the allowed 3-dimensional volume on the plane (m_H, Δ) for electron interacting LDM. The regions have been obtained by marginalizing all the models for each considered scenario (see Sect. 2) and they represent the domain where the likelihood-function values differ more than 10 σ from the *null hypothesis* (absence of modulation). The dashed line ($m_H = \Delta$) marks the case where ν_L is a massless particle. The decay through the detection channel, $\nu_H \to \nu_L e^+ e^-$, is energetically not allowed for the selected configurations. The configurations with $m_H \gtrsim m_e$ (dark area) are interesting for the possible annihilation processes: $\nu_H \bar{\nu}_H \to e^+ e^-$, $\nu_H \bar{\nu}_L \to e^+ e^-$, $\nu_L \bar{\nu}_H \to e^+ e^-$, and $\nu_L \bar{\nu}_L \to e^+ e^-$ in the galactic center. The three nearly vertical curves are the thresholds of these latter processes as mentioned in Ref. [30]. (See color Figure on the journal website.)

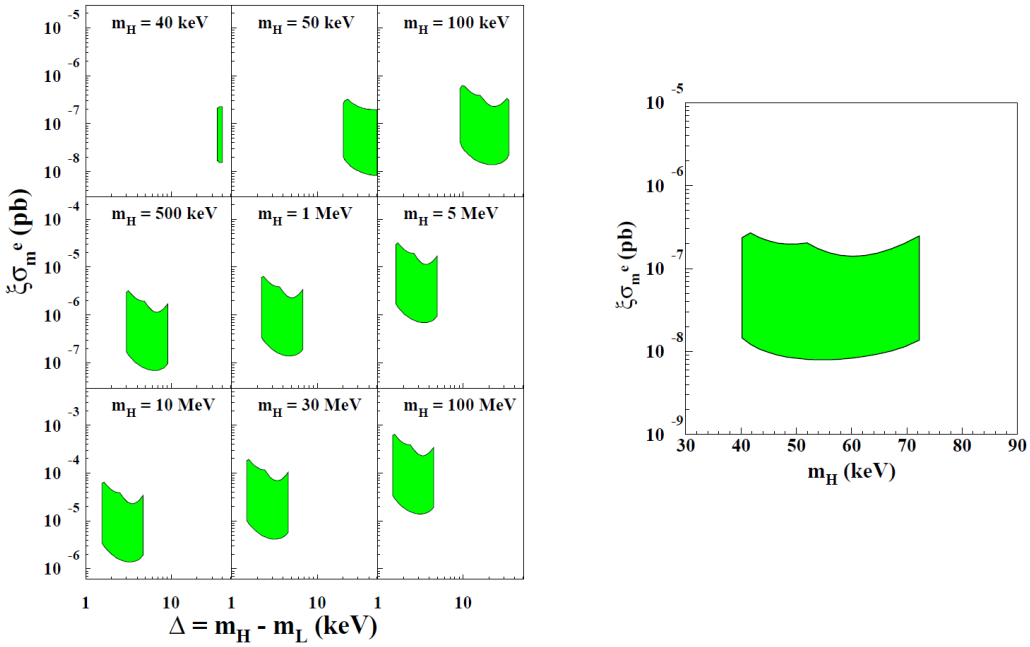

Fig. 22. Case of electron interacting LDM. *Left:* examples of some slices of the allowed 3-dimensional volume for various m_H depicted in the ($\xi\sigma_m^e$ vs Δ) plane at 10 σ from the *null hypothesis* (absence of modulation). *Right*: slice of the allowed 3-dimensional volume at 10 σ from the *null hypothesis* for $m_H = \Delta$, that is for a massless or a very light ν_L particle, as e.g. either an active neutrino or a nearly massless sterile neutrino or the light axion, etc. (See color Figure on the journal website.)

The slice of the allowed 3-dimensional volume for $m_H = \Delta$ at 10 σ from the *null hypothesis* is shown in Fig. 22, *right*. This slice has been taken along the dotted line of Fig. 21, restricting $m_L \simeq 0$, that is for a massless or a very light ν_L particle, such as e.g. either an active neutrino or a nearly massless sterile one or the light axion, etc.

In Fig. 23 an example of superposition of the measured S_m^{exp} vs energy (points with error bars) with theoretical expectation (solid histograms) is shown.

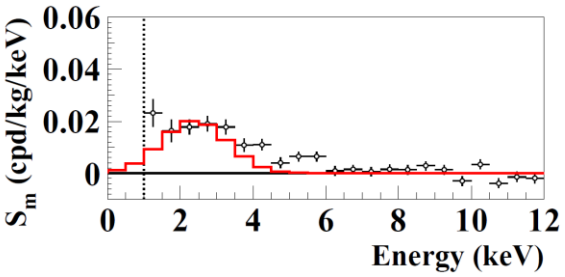

Fig. 23. Example of superposition of the measured S_m^{exp} vs energy (points with error bars) with theoretical expectations (solid histograms) for electron interacting LDM with m_H = 30 MeV, Δ = 2.4 keV and $\xi\sigma_m^e = 1.1\cdot10^{-4}$ pb. The case of the A3 (Evans power-law) halo model with ρ_0 = 0.17 GeV/cm^3 and v_0 = 170 km/s is considered. (See color Figure on the journal website.)

In conclusion, it is worthwhile to summarize that electron interacting LDM candidates in the few-tens-keV/sub-MeV range are allowed by DAMA experiments (see Figs. 21 and 22). This can be of interest, for example, in the models of Warm Dark Matter particles, such as e.g. weakly sterile neutrino.

Moreover, configurations with m_H in the MeV/sub-GeV range are also allowed; similar LDM candidates can also be of interest for the production mechanism of the 511 keV gammas from the galactic bulge.

3.4.2. Interaction with nuclei

With regard to the interaction of LDM with target nuclei, the allowed volume in the space (m_H, Δ, $\xi\sigma_m^{nucleus}$) at 10 σ from the *null hypothesis* can be obtained by comparing the expected modulated signal with the experimental results obtained by DAMA/NaI, DAMA/LIBRA-phase1 and DAMA/LIBRA-phase2 [3 - 7].

The projections of such a region on the plane space (m_H, Δ) are reported in Figs. 24 and 25 for the two above-mentioned illustrative cases of coherent and incoherent nuclear scaling laws, respectively. They have been obtained by marginalizing all the models for each considered scenario (see Sect. 2) and they represent the domain where the likelihood-function values differ more than 10 σ from the *null hypothesis* (absence of modulation).

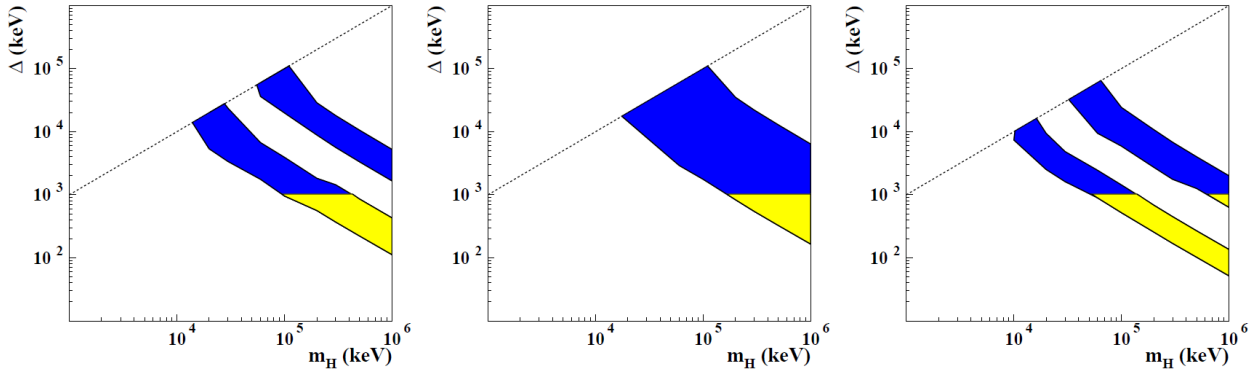

Fig. 24. Case of nucleus interacting LDM. Projections of allowed 3-dimensional volumes on the plane (m_H, Δ) for coherent nuclear scaling law, considering for the quenching factors: (i) Q_I case (*left*), (ii) with channeling effect (*center*), and (iii) Q_{II} (right). The regions have been obtained by marginalizing all the models for each considered scenario (see Sect. 2) and they represent the domain where the likelihood-function values differ more than 10 σ from the *null hypothesis* (absence of modulation). The dashed lines ($m_H = \Delta$) mark the case where ν_L is a massless particle. The decays through the diagram involved in the detection channel are energetically forbidden. (See color Figure on the journal website.)

The allowed m_H values and the splitting Δ are in the intervals 8 MeV $\lesssim m_H \lesssim$ O(GeV)[14] and 29 keV $\lesssim \Delta \lesssim$ 150 MeV, respectively (see Figs. 24 and 25). It is worth noting that in such a case the decays through the diagram involved in the detection channel (e.g. in nucleon anti-nucleon pairs or in meson(s), as $\nu_H \to \nu_L\pi^0$) are obviously energetically forbidden. Moreover, there are allowed configurations that could contribute – in principle, if suitable couplings exist – to the positron generation in the galactic center; in fact, the decay $\nu_H \to \nu_L e^+e^-$ is energetically allowed for $\Delta > 2m_e$ (dark area in Figs. 24 and 25), while the annihilation processes into e^+e^- pairs are energetically allowed for almost all the allowed configurations.

It is worth noting that for nuclear interacting LDM the 3-dimensional allowed configurations are contained in two disconnected volumes, as seen e.g. in their projections in Figs. 24 and 25. The one at larger Δ at m_H fixed is mostly due to interaction on Iodine target, while the other one is mostly due to interaction on Sodium target.

[14] We remind that for m_H values greater than O(GeV) the detection in DAMA experiments would also be possible through the elastic scattering process [15, 16, 26 - 28].

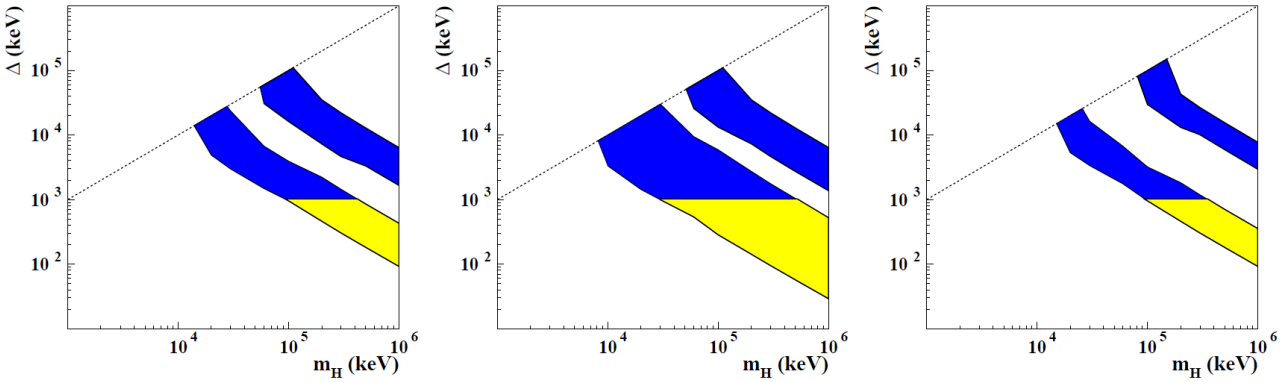

Fig. 25. Case of nucleus interacting LDM. Projections of allowed 3-dimensional volumes on the plane (m_H, Δ) for incoherent nuclear scaling law, considering for the quenching factors: (i) Q_I case (*left*), (ii) with channeling effect (*center*), and (iii) Q_{II} (*right*). The regions have been obtained by marginalizing all the models for each considered scenario (see Sect. 2) and they represent the domain where the likelihood-function values differ more than 10 σ from the *null hypothesis* (absence of modulation). The dashed lines ($m_H = \Delta$) mark the case where ν_L is a massless particle. The decays through the diagram involved in the detection channel are energetically forbidden. (See color Figure on the journal website.)

As examples, some slices of the 3-dimensional allowed volumes for various m_H values in the ($\xi\sigma_m^{coh,inc}$ vs Δ) plane are depicted in Fig. 26 for the two above-mentioned illustrative cases of coherent (*left* panel) and incoherent (*right* panel) nuclear-scaling laws.

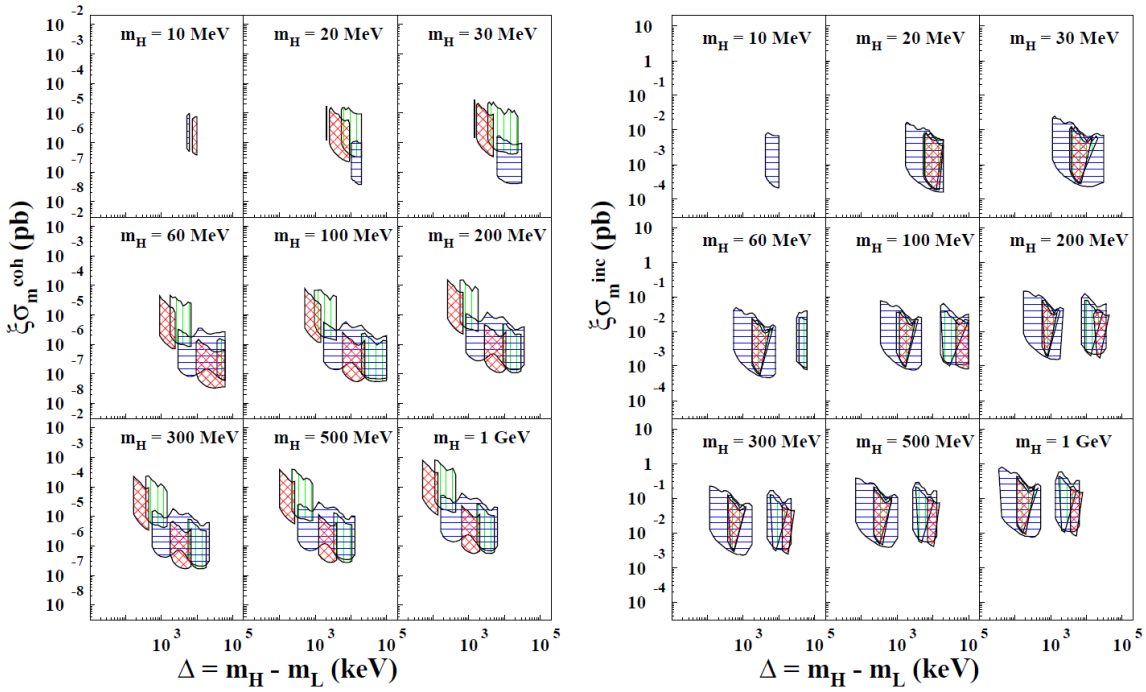

Fig. 26. Case of nucleus interacting LDM. Examples of some slices of the 3-dimensional allowed volumes for various m_H values in the ($\xi\sigma_m^{coh,inc}$ vs Δ) plane for the two illustrative cases of coherent (*left*) and incoherent (*right*) nuclear-scaling laws. Three different instances for the Na and I quenching factors have been considered: (i) Q_I case [(green on-line) vertically-hatched regions], (ii) with channeling effect [(blue on-line) horizontally-hatched regions] and (iii) Q_{II} [(red on-line) cross-hatched regions]. The 3-dimensional volumes have been obtained by marginalizing all the models for each considered scenario (see Sect. 2) and they represent the domain where the likelihood-function values differ more than 10 σ from the *null hypothesis* (absence of modulation). (See color Figure on the journal website.)

The slices of the 3-dimensional allowed volumes for $m_H = \Delta$ are shown in Fig. 27 for the two illustrative cases of coherent (*left* panel) and incoherent (*right* panel) nuclear-scaling laws. These slices have been taken along the dotted lines of Figs. 24 and 25, restricting $m_L \simeq 0$, that is for a massless or a very light ν_L particle, as e.g. either an active neutrino or a nearly massless sterile one or light axion, etc.

In Fig. 28 an example of superposition of the measured S_m^{exp} vs energy (points with error bars) with a theoretical expectation (solid histograms) is shown.

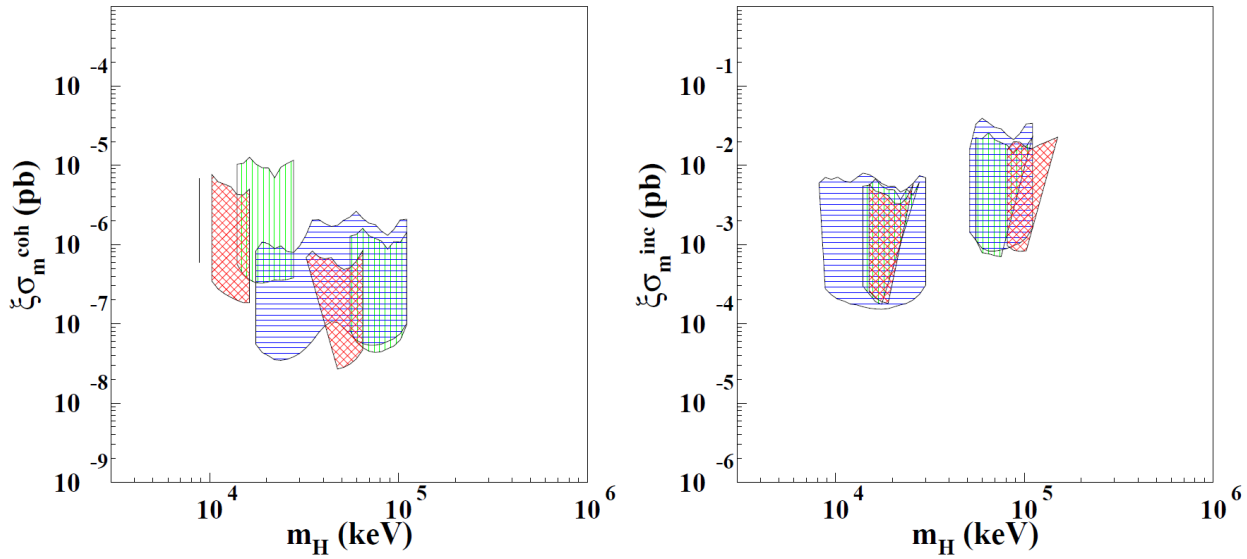

Fig. 27. Case of nucleus interacting LDM. Slices of the 3-dimensional allowed volumes for $m_H = \Delta$, that is for a massless or a very light ν_L particle, as e.g. either an active neutrino or a nearly massless sterile one or the light axion, etc. They are evaluated for the two illustrative cases of coherent (*left* panel) and incoherent (*right* panel) nuclear-scaling laws. Three different instances for the Na and I quenching factors have been considered: (i) Q_I case [(green on-line) vertically-hatched regions], (ii) with channeling effect [(blue on-line) horizontally-hatched regions] and (iii) Q_{II} [(red on-line) cross-hatched regions]. For the coherent case with channeling effect, the low mass region is very narrow so that appears as a vertical segment. The 3-dimensional volumes have been obtained by marginalizing all the models for each considered scenario (see Sect. 2) and they represent the domain where the likelihood-function values differ more than 10 σ from the *null hypothesis* (absence of modulation). (See color Figure on the journal website.)

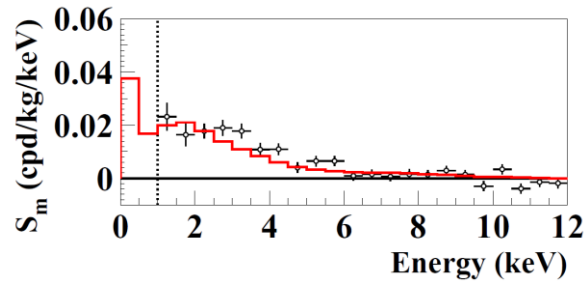

Fig. 28. Example of superposition of the measured S_m^{exp} vs energy (points with error bars) with theoretical expectations (solid histograms) for nucleus interacting LDM with incoherent nuclear scaling law, $m_H = 60$ MeV, $\Delta = 2.9$ MeV and $\xi\sigma_m^{inc} = 3.8 \cdot 10^{-3}$ pb. The case of the C2 (Evans logarithmic) corotating halo model with $\rho_0 = 0.67$ GeV/cm^3 and $v_0 = 170$ km/s is considered. Moreover, the channeling effect is included and the set B of parameter values is used. (See color Figure on the journal website.)

Finally, it is worthwhile to summarize that LDM candidates in the MeV/sub-GeV range are allowed by DAMA experiments (see Figs. 24, 25, 26 and 27). Also, these candidates, such as e.g. axino, sterile neutrino, can be of interest for the positron production in the galactic bulge.

3.5. Mirror Matter

Well-motivated Dark Matter candidates are represented by the so-called Mirror particles. The Mirror scenario can be introduced by considering a parallel gauge sector with particle physics exactly identical to that of ordinary particles, coined as a mirror world. In this theory, the Mirror particles belong to the hidden or shadow gauge sector and can constitute the DM particles of the Universe. A comprehensive discussion about Mirror Matter as DM component can be found in Refs. [20, 21]. In these two papers, in addition, the annual modulation effect measured by DAMA experiments – with lower exposure than presently – has been analyzed in the framework of Asymmetric and Symmetric Mirror Matter scenarios. The following analyses are updated by including the new data of the first six annual cycles of DAMA/LIBRA-phase2 with a lower software energy threshold. This new analysis restricts a significant part of the parameters' space of the Mirror DM scenarios.

3.5.1. Asymmetric Mirror Matter

In the Asymmetric Mirror scenario, the mirror world is a heavier and deformed copy of our world, with mirror particle masses scaled in different ways with respect to the masses of the ordinary particles. Taking the mirror weak scale e.g. of the order of 10 TeV, the mirror electron would become two orders of magnitude heavier than our electron while the mirror nucleons p' and n' only about 5 times heavier than the ordinary nucleons. The dark matter would exist in the form of mirror Hydrogen with the mass of about 5 GeV (which is a rather interesting mass range for DM particles), composed of mirror

proton and electron. The interaction of mirror atomic-type DM candidates with the detector nuclei occurs via the interaction portal which is the kinetic mixing $\frac{\varepsilon}{2}F^{\mu\nu}F'_{\mu\nu}$ of two massless states, ordinary photon, and mirror photon. To fulfill the phenomenology, the mixing parameter is $\varepsilon \ll 1$; this mixing mediates the mirror atom scattering off the ordinary target nuclei in the NaI(Tl) detectors at DAMA/LIBRA set-ups with the Rutherford-like cross-sections.

The low-energy differential cross-section of the interaction between a mirror (A') and ordinary (A) nuclei has the Rutherford-like form:

$$\frac{d\sigma_{A,A'}}{dE_R} = \frac{C_{A,A'}}{E_R^2 v^2}, \qquad (8)$$

where E_R is the energy of the ordinary nucleus recoil, $v = |\mathbf{v}|$ is the relative velocity between the mirror nucleus and the ordinary one, and:

$$C_{A,A'} = \frac{2\pi\varepsilon^2\alpha^2 Z^2 Z'^2}{M_A}\mathbb{F}_A^2\mathbb{F}_{A'}^2, \qquad (9)$$

where α is the fine structure constant, Z and Z's are the charge numbers of the ordinary and mirror nuclei, M_A is the mass of the ordinary nucleus, and $\mathbb{F}_X(qr_X)$ ($X = A, A'$) are the Form-factors of ordinary and mirror nuclei, which depend on the momentum transfer, q, and on the radius of X nucleus.

In the case of asymmetric mirror model, we consider just one species of mirror nuclei. Our benchmark model is the mirror Hydrogen ($A' = Z' = 1$), with mass $M_{A'} \simeq m_p \simeq 5$ GeV (m_p is the proton mass). Alternatively, one can consider the Helium like Δ-atom, with $A' = 1$, $Z' = 2$ and with mass again $M_{A'} \simeq 5$ GeV. For backward compatibility with our previous papers on this subject, the fractional amount of local density in terms of mirror matter is named f only in this Section, instead of the already defined ξ. Hence, the signal rate is proportional to $Z'^2 f\varepsilon^2$. All the numerical results are presented in the case of mirror Hydrogen in terms of $\sqrt{f}\varepsilon$. They would be equivalent to $Z'\sqrt{f}\varepsilon$ in the case of mirror nuclei with $Z' > 1$ with the same mass. So, for Δ-atom one just puts $Z' = 2$.

The data analysis in the Mirror DM model framework considered here allows the determination of the $\sqrt{f}\varepsilon$ parameter. It has been taken into account the uncertainties by marginalizing all the models for each considered scenario (see Sect. 2) for the three instances of the quenching factors: (i) Q_I case, (ii) with channeling effect, and (iii) Q_{II}. The obtained allowed intervals of the $\sqrt{f}\varepsilon$ parameter identify the $\sqrt{f}\varepsilon$ values corresponding to C.L. larger than $10\,\sigma$ from the *null hypothesis*, that is $\sqrt{f}\varepsilon = 0$.

These allowed intervals are: $\sqrt{f}\varepsilon \in [2.28 - 3.13]\cdot 10^{-9}$, and $\sqrt{f}\varepsilon \in [1.19 - 3.38]\cdot 10^{-9}$ for the Q_I and Q_{II} cases, respectively, while no interval is selected for the case when the channeling effect is included. The obtained values of the $\sqrt{f}\varepsilon$ parameter are well compatible with cosmological bounds (see Refs. [20, 21] and references therein).

It is worth noting that in all the considered scenarios for mirror DM the DAMA signal in the 1 - 6 keV energy interval arises mainly from interactions with Sodium nuclei. This effect is due to the fact that the considered Mirror DM particle is quite light: $M_{A'} \simeq 5m_p$.

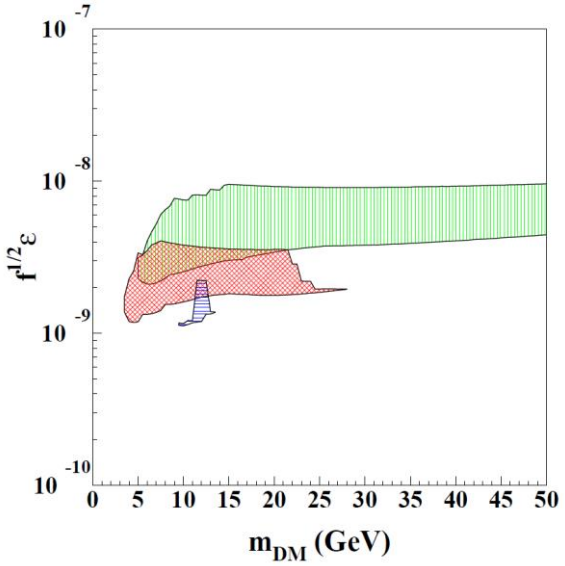

Fig. 29. Regions in the plane $\sqrt{f}\varepsilon$ vs $M_{A'}$ allowed by DAMA experiments in the case of Asymmetric Mirror Matter, when the assumption $M_{A'} \simeq 5m_p$ is released. Three different instances for the Na and I quenching factors have been considered: (i) Q_I case [(green on-line) vertically-hatched region], (ii) with channeling effect [(blue on-line) horizontally-hatched region)] and (iii) Q_{II} [(red on-line) cross-hatched region]. The regions have been obtained by marginalizing all the models for each considered scenario (see Sect. 2) and they represent the domain where the likelihood-function values differ more than $10\,\sigma$ from the *null hypothesis* (absence of modulation).

If the assumption $M_{A'} \simeq 5m_p$ is released, the allowed regions for the $\sqrt{f}\varepsilon$ parameter as a function of $M_{A'}$ ($= m_{DM}$) can be obtained by marginalizing all the models for the three instances for the Na and I quenching factors. This is shown in

Fig. 29 where the m_{DM} interval from few GeV up to 50 GeV is explored. These allowed intervals to identify the $\sqrt{f}\varepsilon$ values corresponding to C.L. larger than $10\,\sigma$ from the *null hypothesis*, that is $\sqrt{f}\varepsilon = 0$. The regions obtained for the three instances for quenching factors can be recognized on the basis of different hatching of the allowed regions.

In Fig. 30 comparisons between the DAMA experimental modulation amplitudes and some expectations for Mirror DM are shown.

Thus, as shown in Figs. 29 and 30, the restrictions on the mirror DM candidate become more severe thanks to the new DAMA/LIBRA-phase2 data (see Ref. [20] for comparison).

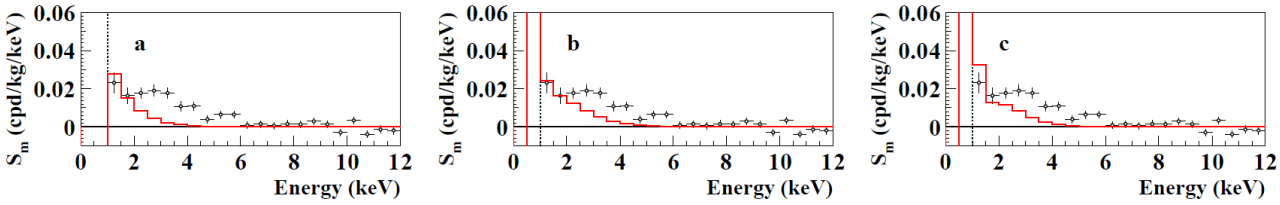

Fig. 30. Examples of superposition of the measured S_m^{exp} vs energy (points with error bars) with theoretical expectations (solid histograms) for Asymmetric Mirror Matter. a – case of the C2 (Evans logarithmic) halo model with $\rho_0 = 0.67$ GeV/cm^3, $v_0 = 170$ km/s, set A of parameters values, $m_{DM} = 11$ GeV, $\sqrt{f}\varepsilon = 1.2\cdot10^{-9}$ including channeling effect; b – case of the C2 (Evans logarithmic) halo model with $\rho_0 = 0.67$ GeV/cm^3, $v_0 = 170$ km/s, set B of parameters values, $m_{DM} = 14$ GeV, $\sqrt{f}\varepsilon = 3.9\cdot10^{-9}$ and quenching Q_I; c – case of the C1 (Evans logarithmic) halo model with $\rho_0 = 0.56$ GeV/cm^3, $v_0 = 170$ km/s, set B of parameters values, $m_{DM} = 7$ GeV, $\sqrt{f}\varepsilon = 2.5\cdot10^{-9}$ and quenching Q_{II}. As can be seen, the data allow discriminating the various scenarios.

3.5.2. Symmetric Mirror Matter

In Symmetric Mirror Matter scenario, the mirror parity exchanging mirror to ordinary particles is an exact symmetry; thus for all ordinary particles: the electron *e*, proton *p*, neutron *n*, photon γ, neutrinos ν etc., with interactions described by the Standard Model $SU(3) \times SU(2) \times U(1)$, there should exist their mirror twins: e', p', n', γ', ν' etc. which are sterile to our strong, weak and electromagnetic interactions but have instead their own gauge interactions $SU(3)' \times SU(2)' \times U(1)'$ with exactly the same coupling constants. Ordinary and mirror particles are degenerate in mass, and the ordinary and mirror sectors have identical microphysics at all levels from particle to atomic physics.

In this context, to analyze the annual modulation observed by DAMA experiments in the framework of Symmetric Mirror Matter, it has been exploited the interaction portal related to the *photon-mirror photon kinetic mixing* term $\frac{\varepsilon}{2}F^{\mu\nu}F'_{\mu\nu}$ with a small parameter $\varepsilon \ll 1$. This mixing renders the mirror nuclei mini-charged with respect to the ordinary electromagnetic force, and thus mediates the scattering of mirror nuclei off ordinary ones with the Rutherford-like cross-sections. The low-energy differential cross-section of the interaction between the mirror and ordinary nuclei has the same form as reported in the previous section. In the Symmetric Scenario, there are different chemical compositions in the mirror sector. The dominant components should be mirror Hydrogen and mirror Helium-4 but a contribution up to a few percents can be due to heavier mirror atoms as Oxygen, Carbon, etc.

In this framework (whose details can be found in Ref. [21]), the Dark Matter particles are expected to form, in the Galaxy, clouds, and bubbles with a diameter which could be as large as the solar system. In this model a dark halo, at the present epoch, is crossing a region close to the Sun with a velocity in the Galactic frame that could be, in principle, arbitrary. Hereafter we will refer to such local bubbles simply as the halo. The halo can be composed of different species of mirror DM particles (different mirror atoms) that have been thermalized and in a frame at rest with the halo. They have a velocity distribution that can be considered Maxwellian with the characteristic velocity related to the temperature of the halo and to the mass of the mirror atoms. We assume that the halo has its own local equilibrium temperature, *T*, and that the velocity parameter of the A' mirror atoms is given by $\sqrt{2k_BT/M_{A'}}$. In this scenario, lighter mirror atoms have larger velocities than the heavier ones, on the contrary to the CDM model where the velocity distribution is mass independent.

It is worthwhile to remind that the expected phase of the annual modulation signal induced by the mirror particles depends on the halo velocity (module and direction) with respect to the laboratory in the Galactic frame. The detailed study of the behavior of the phase in the Symmetric Mirror Model is reported in Ref. [21]. In the data analysis, we have taken into

account all the uncertainties discussed in the previous sections. The scenarios and halo composition described in Ref. [21] have been considered. As an example, in Fig. 31 the expectations of the modulation amplitude calculated for some Symmetric Mirror models favored by DAMA experiments, superimposed to the DAMA experimental modulation amplitudes, are shown.

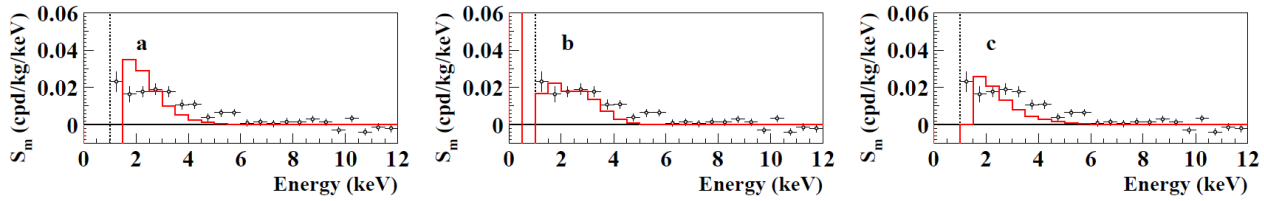

Fig. 31. Examples of superposition of the measured S_m^{exp} vs energy (points with error bars) with theoretical expectations (solid histograms) for Symmetric Mirror Matter for a composite dark halo H′ (24 %), He′(75 %), Fe′(1 %) and $\rho_0 = 0.3$ GeV/cm^3. a – case with $v_0 = 270$ km/s, $v_{halo} = 200$ km/s, $T = 3.1\cdot10^6$ K, parameters in the set A, $\sqrt{f}\varepsilon = 7.1\cdot10^{-10}$ including channeling effect; b – case with $v_0 = 220$ km/s, $v_{halo} = 60$ km/s, $T = 10^5$ K, parameters in the set B, $\sqrt{f}\varepsilon = 2.4\cdot10^{-9}$ and quenching Q_I; c – case with $v_0 = 220$ km/s, $v_{halo} = 100$ km/s, $6.2\cdot T = 10^6$ K, parameters in the set B, $\sqrt{f}\varepsilon = 1.1\cdot10^{-9}$ and quenching Q_{II}. As can be seen, the data allow discriminating the various scenarios.

In the following, the $\sqrt{f}\varepsilon$ values allowed by DAMA experiments in different halo models and some scenarios are reported in order to study how the inclusion of the new data from DAMA/LIBRA-phase2 with 1 keV energy threshold helps to restrict a significant part of the parameters' space. In particular, two different plots for each halo composition are shown: i) allowed regions for the $\sqrt{f}\varepsilon$ parameter as a function of the halo temperature for different values of the halo velocity in the Galactic frame, Fig. 32; ii) allowed regions for the $\sqrt{f}\varepsilon$ parameter as a function of the halo velocity in the Galactic frame for the same temperature $T = 10^4$ K, and for different v_0 values, Fig. 33. The figures refer to two different compositions of halo models. All the reported allowed intervals identify the $\sqrt{f}\varepsilon$ values corresponding to C.L. larger than 10 σ from the *null hypothesis*, that is $\sqrt{f}\varepsilon = 0$.

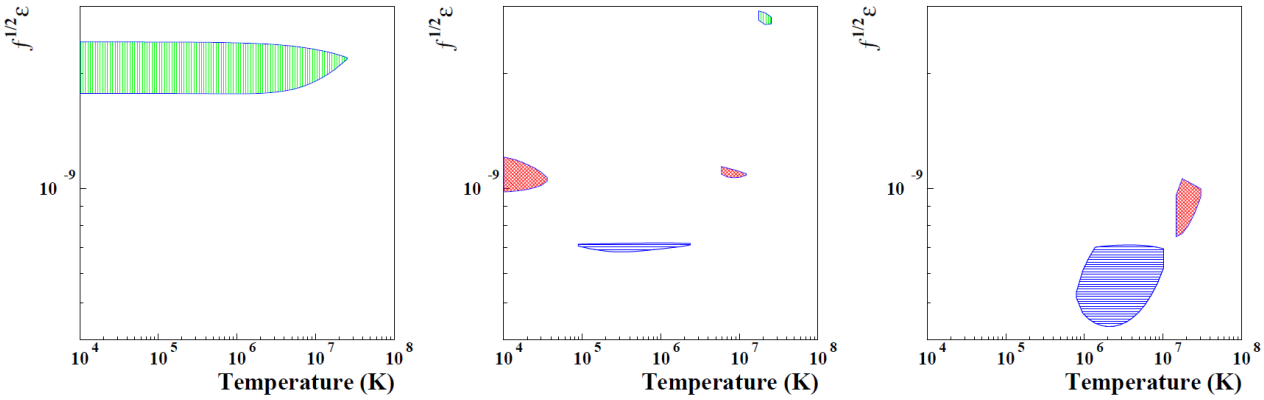

Fig. 32. Some examples of regions in the plane $\sqrt{f}\varepsilon$ vs halo temperature allowed by DAMA experiments in the case of Symmetric Mirror Matter. The regions represent the domain where the likelihood-function values differ more than 10 σ from the *null hypothesis* (absence of modulation). The three graphs refer to different dark halo composition: *Left*: composite dark halo H′(12.5 %), He′(75 %), C′(7 %), O′(5.5 %), with $v_0 = 220$ km/s, $v_{halo} = -100$ km/s and parameters in the set C. *Center*: composite dark halo H′(20 %), He′(74 %), C′(0.9 %), O′(5 %), Fe′(0.1 %), with $v_0 = 220$ km/s, $v_{halo} = 0$ km/s and parameters in the set C. *Right*: composite dark halo H′(24 %), He′(75 %), Fe′(1 %), with $v_0 = 220$ km/s, $v_{halo} = 150$ km/s and parameters in the set C. Three different instances for the Na and I quenching factors have been considered: (i) Q_I case [(green on-line) vertically-hatched regions], (ii) with channeling effect [(blue on-line) horizontally-hatched regions] and (iii) Q_{II} [(red on-line) cross-hatched regions].

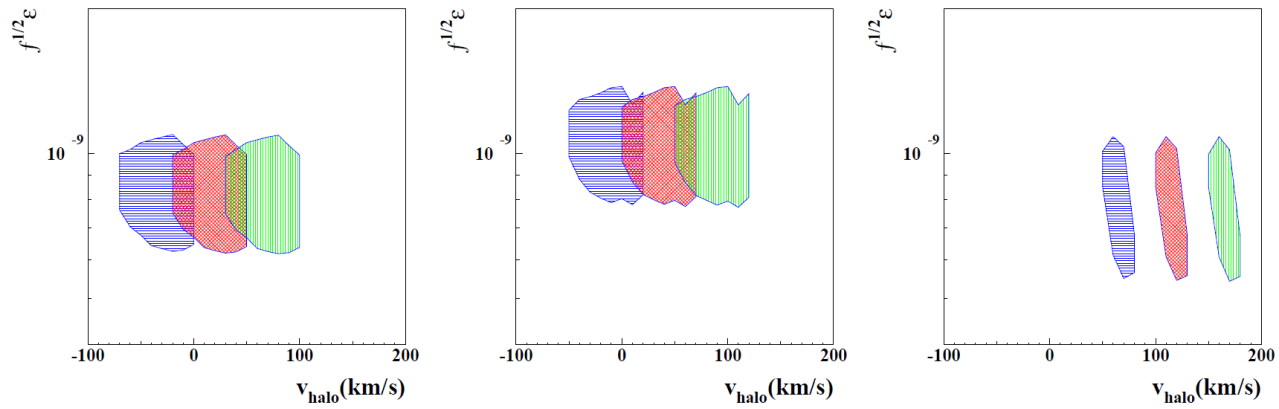

Fig. 33. Regions in the plane $\sqrt{f}\varepsilon$ vs v_{halo} allowed by DAMA experiments in the case of Symmetric Mirror Matter. The regions represent the domain where the likelihood-function values differ more than 10 σ from the *null hypothesis* (absence of modulation). The three graphs refer to different dark halo compositions with the same temperature $T = 10^4$ K, the same set A and the Q_{II} scenario: *Left*: composite dark halo H′(12.5 %), He′(75 %), C′(7 %), O′(5.5 %). *Center*: composite dark halo H′(20 %), He′(74 %), C′(0.9 %), O′(5 %), Fe′(0.1 %). *Right*: composite dark halo H′(24 %), He′(75 %), Fe′(1 %). The three contours in each plot correspond to $v_0 = 170$ km/s [(blue on-line) horizontally-hatched region], $v_0 = 220$ km/s [(red on-line) cross-hatched region] and $v_0 = 270$ km/s [(green on-line) vertically-hatched region].

In conclusion, seemingly the symmetric mirror DM has a better agreement with respect to the asymmetric mirror DM within the considered scenarios. Finally, the mirror DM scenarios are still of interest at the same most stringent C.L. considered for some other scenarios above, and the allowed parameters' space is largely reduced when including the data of the first six annual cycles by DAMA/LIBRA-phase2.

4. Conclusions

The investigation on the nature of the DM particles is an open problem; it always requires a large number of assumptions. In this paper, several possible scenarios for DM candidates are analyzed on the basis of the long-standing DAMA results exploiting the DM annual modulation signature.

In particular, the DAMA/LIBRA-phase2 data, collected over the first six full annual cycles (1.13 t·yr) with a software energy threshold down to 1 keV, are analyzed with the DAMA/NaI and DAMA/LIBRA-phase1 data for several scenarios, improving the confidence levels and restricting the allowed parameters' space of the considered DM candidate particles with respect to previous analyses. For example, in the case of DM particles inducing nuclear recoils through SI elastic scattering low mass candidates are allowed in particular when the channeling effect is included. In the case of a DM candidate with SI isospin violating interaction (that is the effective DM particle couplings to protons and neutrons are not equal), very good agreements are obtained for most of the considered scenarios. Moreover, the cases of a DM candidate with isospin violating interaction and the case of a DM candidate with preferred inelastic interaction including the Thallium contribution are analyzed here by DAMA for the first time.

As shown, in this paper several scenarios are compatible with the observed signal; other possibilities are open as well. In particular, we remind the interest in including tidal stream effects from dwarf satellite galaxies of the Milky Way as e.g. the Sagittarius one (other data from GAIA are expected to add significant information on the topic in near future) or other possible non-thermalized components in the galactic halo as e.g. presence of caustics, as suggested in Ref. [40]. The presence of similar effects could play an important role in the corollary model-dependent results. It is also worth noting that even a suitable particle not yet foreseen by theories may be the- or one-of-the- solution for DM particles. Let us also highlight that in the DM field the case of a single candidate accounting for all DM is generally adopted, as done in the present paper. However, other possibilities exist, as the case of two DM candidates recently proposed to explain the DAMA results [67]. In addition, considering the richness in different particles of the visible matter which is $\ll 1$ % of the Universe density, one could expect that the DM component (about 27 % of the Universe density) may also be multicomponent. This latter possibility is natural in some cases, as e.g. in the mirror DM, as stressed in the present paper.

Similar considerations and the improved results presented in this paper show how important is to improve the capability of the experiment to effectively disentangle among the many possible different scenarios. For such a purpose an increase of exposure in the new lowest energy bins and the lowering of the software energy threshold below

1 keV are important. Thus, DAMA/LIBRA-phase2 has continued its data taking. Moreover, related R&D's towards the so-called phase3 have been funded and are in progress. In particular, new PMTs with high quantum efficiency have been specially developed by HAMAMATSU: R11065-20MOD, which satisfy all the needed requirements, and a new voltage divider allocating the preamplifier on the same basis has been designed and already tested.

In conclusion, the new data have allowed significantly improving the confidence levels and restricting the allowed parameters' space for the various considered scenarios with respect to previous DAMA analyses; efforts towards further improvements are in progress.

REFERENCES

1. R. Bernabei et al. Performances of the new high quantum efficiency PMTs in DAMA/LIBRA. J. Instrum. 7 (2012) P03009.
2. R. Bernabei et al. Dark matter investigation by DAMA at Gran Sasso. Int. J. Mod. Phys. A 28 (2013) 1330022.
3. R. Bernabei et al. First Model Independent Results from DAMA/LIBRA-Phase2. Universe 4 (2018) 116.
4. R. Bernabei et al. New Model Independent Results From the First Six Full Annual Cycles of DAMA/LIBRA-phase2. Bled Workshops in Physics 19 n. 2 (2018) 27.
5. R. Bernabei et al. First model independent results from DAMA/LIBRA-phase2. Nucl. Phys. At. Energy 19 (2018) 307.
6. R. Bernabei et al. First results from DAMA/LIBRA-phase2. Nuclear and Particle Physics Proceed. 303-305 (2018) 74.
7. R. Bernabei et al. In the Proc. of 15-th Marcel Grossmann Meeting (World Sci., Singapore, 2019).
8. R. Bernabei et al. The DAMA/LIBRA apparatus. Nucl. Instr. Meth. A 592 (2008) 297.
9. R. Bernabei et al. First results from DAMA/LIBRA and the combined results with DAMA/NaI. Eur. Phys. J. C 56 (2008) 333.
10. R. Bernabei et al. New results from DAMA/LIBRA. Eur. Phys. J. C 67 (2010) 39.
11. R. Bernabei et al. Final model independent result of DAMA/LIBRA-phase1. Eur. Phys. J. C 73 (2013) 2648.
12. R. Bernabei et al. No role for muons in the DAMA annual modulation results. Eur. Phys. J. C 72 (2012) 2064.
13. R. Bernabei et al. No role for neutrons, muons and solar neutrinos in the DAMA annual modulation results. Eur. Phys. J. C 74 (2014) 3196.
14. DAMA coll. issue dedicated to DAMA. Int. J. of Mod. Phys. A 31 (2016) and Refs therein.
15. R. Bernabei el al. Dark matter search. La Rivista del Nuovo Cimento 26(1) (2003) 1 and Refs. therein.
16. R. Bernabei et al. Dark matter particles in the galactic halo: Results and implications from DAMA/NaI. Int. J. Mod. Phys. D 13 (2004) 2127 and Refs. therein.
17. K.A. Drukier et al. Detecting cold dark-matter candidates. Phys. Rev. D 33 (1986) 3495.
18. K. Freese et al. Signal modulation in cold-dark-matter detection. Phys. Rev. D 37 (1988) 3388.
19. P. Belli et al. Observations of annual modulation in direct detection of relic particles and light neutralinos. Phys. Rev. D 84 (2011) 055014.
20. A. Addazi et al. DAMA annual modulation effect and asymmetric mirror matter. Eur. Phys. J. C 75 (2015) 400.
21. R. Cerulli et al. DAMA annual modulation and mirror dark matter. Eur. Phys. J. C 77 (2017) 83.
22. P. Belli et al. Extending the DAMA annual modulation region by inclusion of the uncertainties in astrophysical velocities. Phys. Rev. D 61 (2000) 023512.
23. R. Bernabei et al. Investigating the DAMA annual modulation data in the framework of inelastic dark matter. Eur. Phys. J. C 23 (2002) 61.
24. P. Belli et al. Effect of the galactic halo modeling on the DAMA-NaI annual modulation result: An extended analysis of the data for weakly interacting massive particles with a purely spin-independent coupling. Phys. Rev. D 66 (2002) 043503.
25. R. Bernabei et al. Investigating pseudoscalar and scalar dark matter. Int. J. Mod. Phys. A 21 (2006) 1445.
26. R. Bernabei et al. Investigating halo substructures with annual modulation signature. Eur. Phys. J. C 47 (2006) 263.
27. R. Bernabei et al. On electromagnetic contributions in WIMP quests. Int. J. Mod. Phys. A 22 (2007) 3155.
28. R. Bernabei et al. Possible implications of the channeling effect in NaI(Tl) crystals. Eur. Phys. J. C 53 (2008) 205.
29. R. Bernabei et al. Investigating electron interacting dark matter. Phys. Rev. D 77 (2008) 023506.
30. R. Bernabei et al. Investigation on light dark matter. Mod. Phys. Lett. A 23 (2008) 2125.
31. A.M. Green. Astrophysical uncertainties on the local dark matter distribution and direct detection experiments. J. Phys. G 44 (2017) 084001.
32. N.W. Evans, C.A.J. O'Hare, C. McCabe. Refinement of the standard halo model for dark matter searches in light of the Gaia Sausage. Phys. Rev. D 99 (2019) 023012.
33. A.J. Deason et al. The local high-velocity tail and the Galactic escape speed. Mon. Not. R. Astron. Soc. 485 (2019) 3514.

34. M.C. Smith et al. The RAVE survey: constraining the local Galactic escape speed. Mon. Not. R. Astron. Soc. 379 (2007) 755.
35. T. Piffl et al. The RAVE survey: the Galactic escape speed and the mass of the Milky Way. Astronomy & Astrophysics 562 (2014) A91.
36. A.A. Williams et al. On the run: mapping the escape speed across the Galaxy with SDSS. Mon. Not. R. Astron. Soc. 468 (2017) 2359.
37. G. Monari et al. The escape speed curve of the Galaxy obtained from *Gaia* DR2 implies a heavy Milky Way. Astronomy & Astrophysics 616 (2018) L9.
38. K. Freese et al. Detectability of weakly interacting massive particles in the Sagittarius dwarf tidal stream. Phys. Rev. D 71 (2005) 043516.
39. K. Freese et al. Effects of the Sagittarius dwarf tidal stream on dark matter detectors. Phys. Rev. Lett. 92 (2004) 111301.
40. F.S. Ling, P. Sikivie, S. Wick. Diurnal and annual modulation of cold dark matter signals. Phys. Rev. D 70 (2004) 123503.
41. P. Gondolo et al. DarkSUSY 4.00 neutralino dark matter made easy. New Astron. Rev. 49 (2005) 193.
42. G. Gelmini, P. Gondolo. Weakly interacting massive particle annual modulation with opposite phase in late-infall halo models. Phys. Rev. D 64 (2001) 023504.
43. D.N. Spergel, P.J. Steinhardt. Observational Evidence for Self-Interacting Cold Dark Matter. Phys. Rev. Lett. 84 (2000) 3760.
44. B.D. Wandelt et al. Self-Interacting Dark Matter. Proc. 4th Int. Symp. "Sources and Detection of Dark Matter and Dark Energy in the Universe" (Springer, Berlin, 2001) p. 263.
45. H.W. Joo et al. Quenching factor measurement for NaI(Tl) scintillation crystal. Astropart. Phys. 108 (2019) 50.
46. G. Adhikari et al. Initial performance of the COSINE-100 experiment. Eur. Phys. J. C 78 (2018) 107.
47. D.R. Tovey et al. Measurement of scintillation efficiencies and pulse-shapes for nuclear recoils in NaI(Tl) and CaF_2(Eu) at low energies for dark matter experiments. Phys. Lett. B 433 (1998) 150.
48. J. Xu et al. Scintillation efficiency measurement of Na recoils in NaI(Tl) below the DAMA/LIBRA energy threshold. Phys. Rev. C 92 (2015) 015807.
49. R. Bernabei et al. New limits on WIMP search with large-mass low-radioactivity NaI(Tl) set-up at Gran Sasso. Phys. Lett. B 389 (1996) 757.
50. V.I. Tretyak. Semi-empirical calculation of quenching factors for ions in scintillators. Astropart. Phys. 33 (2010) 40.
51. J.I. Collar. Quenching and channeling of nuclear recoils in NaI(Tl): Implications for dark-matter searches. Phys. Rev. C 88 (2013) 035806.
52. S.I. Matyukhin. Critical parameters of channeling. Tech. Phys. 53 (2008) 1578.
53. N. Bozorgnia et al. Channeling in direct dark matter detection I: channeling fraction in NaI(Tl) crystals. J. Cosmol. Astropart. Phys. 11 (2010) 019.
54. R. Bernabei et al. Investigating the DAMA annual modulation data in a mixed coupling framework. Phys. Lett. B 509 (2001) 197.
55. G. Prezeau et al. New Contribution to Scattering of Weakly Interacting Massive Particles on Nuclei. Phys. Rev. Lett. 91 (2003) 231301.
56. R.H. Helm. Inelastic and Elastic Scattering of 187-Mev Electrons from Selected Even-Even Nuclei. Phys. Rev. 104 (1956) 1466.
57. J.D. Lewin, P.F. Smith. Review of mathematics, numerical factors, and corrections for dark matter experiments based on elastic nuclear recoil. Astropart. Phys. 6 (1996) 87.
58. S. Baum, K. Freese, C. Kelso. Dark Matter implications of DAMA/LIBRA-phase2 results. Phys. Lett. B 789 (2019) 262.
59. S. Kang et al. DAMA/LIBRA-phase2 in WIMP effective models. J. Cosmol. Astropart. Phys. 07 (2018) 016.
60. F. Kahlhoefer et al. Model-independent comparison of annual modulation and total rate with direct detection experiments. J. Cosmol. Astropart. Phys. 05 (2018) 074.
61. D. Smith, N. Weiner. Inelastic dark matter. Phys. Rev. D 64 (2001) 043502.
62. D. Tucker-Smith, N. Weiner. Status of inelastic dark matter. Phys. Rev. D 72 (2005) 063509.
63. D.P. Finkbeiner et al. Inelastic dark matter and DAMA/LIBRA: An experimentum crucis. Phys. Rev. D 80 (2009) 115008.
64. S. Kang et al. Proton-philic spin-dependent inelastic dark matter as a viable explanation of DAMA/LIBRA-phase2. Phys. Rev. D 99 (2019) 023017.
65. S. Kang, S. Scopel, G. Tomar. Probing DAMA/LIBRA in the full parameter space of WIMP effective models of inelastic scattering. Phys. Rev. D 99 (2019) 103019.
66. S. Chang, R.F. Lang, N. Weiner. Effect of Thallium Impurities in the DAMA Experiment on the Allowed Parameter Space for Inelastic Dark Matter. Phys. Rev. Lett. 106 (2011) 011301.
67. J. Herrero-Garcia et al. Time-dependent rate of multicomponent dark matter: Reproducing the DAMA/LIBRA phase-2 results. Phys. Rev. D 98 (2018) 123007.

Р. Бернабей[1,2,*], П. Беллі[1,2], Ф. Капелла[3,4], В. Караччіоло[5], Р. Черуллі[1,2], Ц. Ж. Дай[6], А. д'Анджело[3,4], А. Ді Марко[2], Х. Л. Хе[6], А. Інчікітті[3,4], І. Х. Ма[6], В. Мерло[1,2], Ф. Монтеккі[2,7], І. Д. Шенг[6], З. П. Йе[6,8]

[1] Фізичний факультет, Римський університет «Тор Вергата», Рим, Італія
[2] Національний інститут ядерної фізики, відділення у Римі «Тор Вергата», Рим, Італія
[3] Фізичний факультет, Римський університет «Ла Сапієнца», Рим, Італія
[4] Національний інститут ядерної фізики, відділення у Римі, Рим, Італія
[5] Національна лабораторія Гран-Сассо, Ассерджі, Італія
[6] Ключова лабораторія астрофізики частинок, Інститут фізики високих енергій, Китайська академія наук, Пекін, КНР
[7] Факультет цивільної інженерії та інформатики, Римський університет «Тор Вергата», Рим, Італія
[8] Університет Цзінганшань, Цзянь, Цзянси, КНР

*Відповідальний автор: rita.bernabei@roma2.infn.it

ВДОСКОНАЛЕНИЙ МОДЕЛЬНО-ЗАЛЕЖНИЙ АНАЛІЗ ПАРАМЕТРІВ ТЕМНОЇ МАТЕРІЇ ПІСЛЯ ПЕРШИХ ШЕСТИ РІЧНИХ ЦИКЛІВ В ЕКСПЕРИМЕНТІ DAMA/LIBRA-phase2

Деякі з багатьох запропонованих кандидатів на роль частинок Темної Матерії, вже досліджені з меншою експозицією та більш високим порогом енергії, аналізуються додатково з включенням перших даних експерименту DAMA/LIBRA-phase2 із експозицією 1,13 т·рік та нижчим енергетичним порогом (1 кеВ). Загальна експозиція з порогом 2 кеВ, враховуючи також дані DAMA/NaI та DAMA/LIBRA-phase1, зараз становить 2,46 т·рік. Аналіз дозволяє обмежити простір параметрів для розглянутих кандидатів, звужуючи їх значення – порівняно з попередніми аналізами – завдяки збільшенню експозиції та нижчому порогу енергії.

Ключові слова: темна матерія, WIMP, процеси з елементарними частинками, сцинтиляційні детектори.

Р. Бернабей[1,2,*], П. Белли[1,2], Ф. Капелла[3,4], В. Караччиоло[5], Р. Черулли[1,2], Ц. Ж. Дай[6], А. д'Анджело[3,4], А. Ди Марко[2], Х. Л. Хе[6], А. Инчикитти[3,4], И. Х. Ма[6], В. Мерло[1,2], Ф. Монтекки[2,7], И. Д. Шенг[6], З.П. Йе[6,8]

[1] Физический факультет, Римский университет «Тор Вергата», Рим, Италия
[2] Национальный институт ядерной физики, отделение в Риме «Тор Вергата», Рим, Италия
[3] Физический факультет, Римский университет «Ла Сапиенца», Рим, Италия
[4] Национальный институт ядерной физики, отделение в Риме, Рим, Италия
[5] Национальная лаборатория Гран-Сассо, Ассерджи, Италия
[6] Ключевая лаборатория астрофизики частиц, Институт физики высоких энергий, Китайская академия наук, Пекин, КНР
[7] Ф-т гражданской инженерии и информатики, Римский университет "Тор Вергата", Рим, Италия
[8] Университет Цзинганшань, Цзянь, Цзянси, КНР

Ответственный автор: rita.bernabei@roma2.infn.it

УЛУЧШЕННЫЙ МОДЕЛЬНО-ЗАВИСИМЫЙ АНАЛИЗ ПАРАМЕТРОВ ТЕМНОЙ МАТЕРИИ ПОСЛЕ ПЕРВЫХ ШЕСТИ ГОДОВЫХ ЦИКЛОВ В ЭКСПЕРИМЕНТЕ DAMA/LIBRA-phase2

Некоторые из многих предложенных кандидатов на роль частиц Темной Материи, уже исследованные с меньшей экспозицией и более высоким порогом энергии, анализируются дополнительно с включением первых данных эксперимента DAMA/LIBRA-phase2 с экспозицией 1,13 т·год и более низким энергетическим порогом (1 кэВ). Общая експозиция с порогом 2 кэВ, включая также данные DAMA/NaI и DAMA/LIBRA-phase1, сейчас составляет 2,46 тонн × год. Анализ позволяет ограничить пространство параметров для рассмотренных кандидатов, сужая их значения – сравнительно с предыдущими анализами – благодаря увеличению экспозиции и более низкому порогу энергии.

Ключевые слова: темная материя, WIMP, процессы с элементарными частицами, сцинтилляционные детекторы.

Надійшла 23.08.2019
Received 23.08.2019